Contract No:

This document was prepared in conjunction with work accomplished under Contract No. DE-AC09-08SR22470 with the U.S. Department of Energy (DOE) Office of Environmental Management (EM).

Disclaimer:

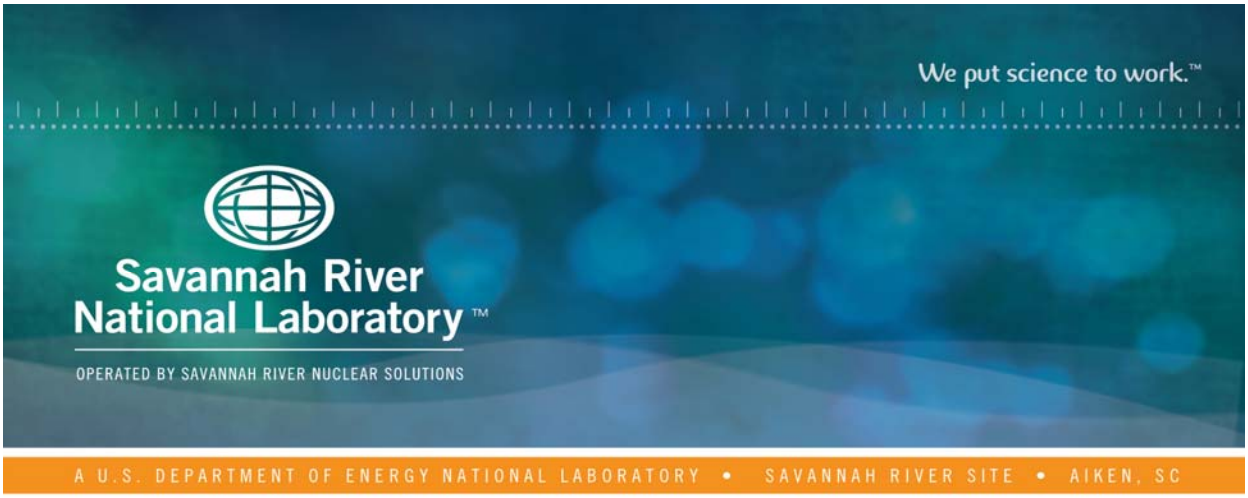

SME ACCEPTABILITY DETERMINATION FOR DWPF PROCESS CONTROL (U)

Thomas B. Edwards

June 2017

WSRC-TR-95-00364 Revision 6

DISCLAIMER

Printed in the United States of America

Prepared for
U.S. Department of Energy

Keywords: : **statistics, statistical process control, MFT, Melter, PCCS**

Retention: Permanent

SME ACCEPTABILITY DETERMINATION FOR DWPF PROCESS CONTROL (U)

Thomas B. Edwards

June 2017

Prepared for the U.S. Department of Energy under contract number DE-AC09-08SR22470.

Savannah River National Laboratory™
OPERATED BY SAVANNAH RIVER NUCLEAR SOLUTIONS

REVIEWS AND APPROVALS

AUTHOR:

T.B. Edwards, Immobilization Technology Date

TECHNICAL REVIEW:

F.C. Johnson, Immobilization Technology Date

K.M. Fox, Waste Form Processing Technologies, Reviewed per E7 2.60 Date

APPROVAL:

S.D. Fink, Manager Date
SRNL Support for Salt Waste Processing Facility

D.E. Dooley, Director Date
Chemical Processing Technologies

E.J. Freed, Manager Date
Defense Waste Processing Facility and Saltstone Facility Engineering

ACKNOWLEDGEMENTS

The statistical system described in this document is called the Product Composition Control System (PCCS). K. G. Brown and R. L. Postles were the originators and developers of this system as well as the authors of the first three versions of this technical basis document for PCCS. PCCS has guided acceptability decisions for the processing at the Defense Waste Processing Facility (DWPF) at the Savannah River Site (SRS) since the start of radioactive operations in 1996. The author of this revision to the document gratefully acknowledges the firm technical foundation that Brown and Postles established to support the ongoing successful operation at the DWPF. Their integration of the glass property-composition models, developed under the direction of C. M. Jantzen, into a coherent and robust control system, has served the DWPF well over the last 20^{+} years, even as new challenges, such as the introduction into the DWPF flowsheet of auxiliary streams from the Actinide Removal Process (ARP) and other processes, were met.

The purpose of this revision is to provide a technical basis for modifications to PCCS required to support the introduction of waste streams from the Salt Waste Processing Facility (SWPF) into the DWPF flowsheet. An expanded glass composition region is anticipated by the introduction of waste streams from SWPF, and property-composition studies of that glass region have been conducted. Jantzen, once again, directed the development of glass property-composition models applicable for this expanded composition region. The author gratefully acknowledges the technical contributions of C.M. Jantzen leading to the development of these glass property-composition models. The integration of these models into the PCCS constraints necessary to administer future acceptability decisions for the processing at DWPF is provided by this sixth revision of this document.

PREFACE

This document has supported the technical basis for the Defense Waste Processing Facility (DWPF) since start of radioactive operation in 1996. The facility blends High Level Waste (HLW) with glass frit and vitrifies the resulting mix into a stable, borosilicate waste form. While doing so, the facility must satisfy, with appropriate confidence, several product and process constraints. These include constraints on:

- the process melt (i.e., melt viscosity and liquidus temperature) to assure that the material is process-able, and
- the quality of the resulting waste form (i.e., durability of the glass product).

DWPF personnel cannot wait until the melt or waste glass has been made to assess its acceptability, since by then no changes to either are possible. Therefore, the acceptability decision is made on the upstream process, rather than on the downstream melt or glass product. That is, the decision is based on statistical process control rather than statistical quality control.

The decision as to whether a particular process slurry feed batch (containing sludge, frit, and possibly salt product streams) will produce a melt (and thus glass) that satisfies the aforementioned constraints is necessarily based on sampling and measurement. These samples and measurements are uncertain because of random and systematic "errors" of various kinds, and the acceptability decision must be made in the face of these uncertainties. It is, accordingly, a statistical decision. The acceptability decision is described in this document, and a statistical system is developed to adjudge whether, after allowing for appropriate uncertainties, the relevant measurements and projections are sufficiently distant from the constraints to be acceptable. The statistical system is called the Product Composition Control System (PCCS).

The glass and melt properties that must be controlled have been related through statistical models to glass composition, which is, in turn, dictated by feed slurry composition. Accordingly, the PCCS strategy is to blend and then monitor the composition of the feed slurry in the Slurry Mix Evaporator (SME). The SME is both the first control point in the DWPF process wherein all necessary constituents are present and the last control point at which any change to them can be effected. The PCCS thus deals with monitoring the blended SME batch.

Uncertainties exist within all DWPF operations. These uncertainties affect all steps of, and all samples and measurements on, the process. They affect the collection of slurry samples, the preparation of these samples for measurement, and the measurements themselves. Uncertainty is also present in the property-composition models.

The aggregate of all this uncertainty motivates the use of the PCCS. The PCCS enables rational, high-confidence decisions concerning acceptability by accounting for uncertainty in a methodical, logical, and quantitative way.

Thus, the main focus of PCCS is to monitor an extant SME batch to see whether it is acceptable prior to its being transferred to the melter. The purpose of this report is to provide the technical basis for PCCS.

EXECUTIVE SUMMARY

This document establishes the technical basis for Defense Waste Processing Facility's (DWPF's) Product Composition Control System (PCCS), a statistical process control system for monitoring Slurry Mix Evaporator (SME) batches and for supporting acceptability decisions at this production hold-point for the facility. Using chemical composition measurements derived from SME samples as input, the system assesses the acceptability of the SME batch against appropriate process, product quality, and solubility constraints after accounting for applicable uncertainties (i.e., those due to property models, when such models are used, and those due to the sample measurements themselves).

This is the sixth revision of the SME Acceptability Determination report, and it establishes the technical basis necessary for the modification of PCCS that is to occur prior to the integration of the Salt Waste Processing Facility (SWPF) into the DWPF flowsheet.

TABLE OF CONTENTS

LIST OF TABLES

LIST OF FIGURES

LIST OF ABBREVIATIONS

ARP	Actinide Removal Process
ccc	Centerline canister cooled
CELS	Corning Engineering Laboratory Services
DWPF	Defense Waste Processing Facility
D&S-FE	DWPF & Saltstone Facility Engineering
EA	Environmental Assessment (glass)
EPAR	Expected Property Acceptance Region
HLW	High Level Waste
LWO	Liquid Waste Organization
MAR	Measurement Acceptance Region
MFT	Melter Feed Tank
MU	Measurement Uncertainty
P	Poise
PAR	Property Acceptance Region
PCCS	Product Composition Control System
PCT	Product Consistency Test
ppm	Parts per million
REDOX	Reduction/Oxidation
RMSE	Root Mean Square Error
ROC	Reduction of Constraints
SB#	Sludge Batch (number #)
SME	Slurry Mix Evaporator
SRAT	Sludge Receipt and Adjustment Tank
SRNL	Savannah River National Laboratory
SRR	Savannah River Remediation
SRS	Savannah River Site
SWPF	Salt Waste Processing Facility
T_L	Liquidus Temperature
TTQAP	Task Technical and Quality Assurance Plan
TTR	Technical Task Request
WAPS	Waste Acceptance Product Specifications
wt%	Weight percent

1.0 Introduction

The Defense Waste Processing Facility (DWPF) at the Savannah River Site (SRS) in Aiken, South Carolina, began immobilizing high level waste (HLW) in borosilicate glass in 1996. For its HLW immobilization to be successful, the facility must consistently obey several product and process constraints including those related to melt viscosity and liquidus temperature (i.e., the process-ability of the material being vitrified) and to glass durability (i.e., the quality of the resulting waste form product). The process and product properties are assessed through models that relate each of the properties to the chemical composition of the glass, which is determined from measurements of in-process samples taken on each process batch at the Slurry Mix Evaporator (SME) tank. A set of waste solubility constraints on the resulting glass product also must be satisfied.

The system used by the DWPF to assess the performance of a process batch against the applicable constraints is called the Product Composition Control System (PCCS). The PCCS guides the acceptability decision for each DWPF process batch. This report, in its earlier versions, has served as the technical basis for that system since the beginning of radioactive operations. The report is being revised to implement key modifications to the acceptability decision at the DWPF necessary for the integration of waste streams from the Salt Waste Processing Facility (SWPF) into the DWPF flowsheet. The major modifications are the implementation of a new viscosity model, new durability models, and a new liquidus temperature model. Other modifications include the revision of the upper limit, no longer a solubility limit, for TiO_2 in the glass, revisions of the limits on the durability constraints, and modifications to the reduction of constraints associated with maintaining control over the homogeneity of the glass waste form. The revision of this report has been guided by a Task Technical and Quality Assurance plan (TTQAP) [1], which was prepared in response to a Technical Task Request (TTR) [2].

This report is organized as follows. The requirements for quality assurance associated with this report are addressed in the next section. Section 3 provides an overview of the strategy supporting the SME acceptability decisions. Section 4 specifies the original constraints imposed on the DWPF operations, identifies the associated categories of uncertainties that must be accounted for, and establishes the corresponding levels of confidence. In Section 5, the alternatives implemented in Revision 4 of this report to satisfy the DWPF's original constraints are outlined and their influence on the control strategy is discussed. A modification to the type of TiO_2 limit introduced in this revision is also discussed in this section. Section 6 provides a detailed, systematic discussion of each of the constraints including property model uncertainty and measurement uncertainty (MU). A new viscosity model, new durability models, a new liquidus temperature model, and other modifications including the revision of the upper limit for TiO_2 (no longer a solubility limit but now a model applicability limit), and modifications to the reduction of constraints associated with maintaining control over the homogeneity of the glass waste form are included as part of the discussion in Section 6. Section 7 discusses issues associated with reduction/oxidation (REDOX). Section 8 provides a sample calculation to illustrate the use of PCCS. The final sections provide a discussion of recommendations and conclusions. The appendices provide additional details and discussion supporting the PCCS calculations.

2.0 Quality Assurance

Requirements for performing reviews of technical reports and the extent of review are established in manual E7 2.60. SRNL documents the extent and type of review using the SRNL Technical Report Design Checklist contained in WSRC-IM-2002-00011, Rev. 2. The focus of this review was to confirm the updates needed in this revision to reflect the changes to the property models and their uncertainties.

3.0 Overview of the Control Strategy

In the DWPF, radioactive sludge is transferred into the Sludge Receipt and Adjustment Tank (SRAT) to begin a process batch. Auxiliary streams such as those anticipated from SWPF are added to the SRAT during the processing of that tank, and the SRAT product is transferred to the SME. Ground glass (frit) is blended with the contents of the SME to produce melter feed slurry. From here, the material then passes to the Melter Feed Tank (MFT), which continuously feeds the melter. The melter vitrifies the feed slurry into a molten glass waste form, which is poured into stainless steel canisters for cooling and ultimate storage.

DWPF personnel cannot wait until the melt or waste glass has been made to assess its acceptability, since by then no changes to either are possible. Therefore, the acceptability decision is made on the upstream process, rather than on the downstream melt or glass product. That is, the decision is based on statistical process control rather than statistical quality control, and the acceptability decision is made at the SME. The SME is uniquely positioned in the process — it is both the first control point in the process wherein all necessary constituents are present and the last control point at which any change to them can be effected. Thus, the control strategy involves monitoring the blended SME batch.

Monitoring of the SME is accomplished by sampling its contents. For each SME batch, a set of ($n \geq 4$) samples is taken to initiate an acceptability decision. Each of these samples is vitrified and the chemical compositions of the resulting n glasses are measured. The average of the measured chemical compositions for a minimum of 4 samples is determined (see Appendix A for a description of the sample measurements), and this average composition serves as the basis for the acceptability decision for the SME batch.

However, the average chemical composition, while necessary, is not sufficient in and of itself, to complete the assessment of the performance of the SME contents against the constraints. Some of the constraints involve properties (either process or product quality) such as viscosity, liquidus temperature, and durability. These properties cannot be measured in situ, and thus, they must be predicted from models that relate these properties to glass composition. Not only must the model predictions satisfy their corresponding property constraints, but the constraints must also be appropriately met after the applicable modeling uncertainties are introduced into the acceptability decision.

For the constraints involving property-composition models and for most of the other constraints that directly involve composition, the uncertainties associated with the SME samples must also be accounted for as part of the acceptability decision. The uncertainties, labeled MUs in this report, include those related to the collection of the slurry samples in the SME, the preparation of these samples for measurement, and the measurements themselves.

A glass composition representing the “average” content of a SME batch is deemed to be within the acceptable operating window for the DWPF if all of the applicable constraints are satisfied, at appropriate confidence levels, after all of the related property modeling uncertainties and MUs

are accounted for. Conceptually, there is a layered approach to the acceptability decision. At the first step, the question is, does the average chemical composition representing the SME contents directly or through model predictions satisfy the constraints? If the answer is yes, the composition is said to be within the Expected Property Acceptance Region (EPAR). However, the EPAR does not account for uncertainties in the predicting models. If, after the property model uncertainties are accounted for (to be discussed later), the chemical composition still meets the constraints, then the composition is said to be within the Property Acceptance Region (PAR). Finally, if, after measurement uncertainties are accounted for (to be discussed later), the chemical composition still meets the constraints, then the composition is said to be within the Measurement Acceptance Region (MAR). A composition that is within the MAR for each of the applicable constraints is also within the PAR and EPAR for these constraints. Such a composition is said to be within the acceptable operating window of the DWPF, and thus, the associated SME material can be transferred to the MFT and ultimately the melter.

As mentioned earlier, some of the constraints are directly related to composition and do not involve model predictions. For these constraints fewer layers in the above description apply. Specifically, the PAR limits would be the same as the EPAR limits for such constraints since there is no property model uncertainty. In a similar fashion, if there is no need to apply property modeling uncertainty or MU for a given constraint (which is true for a pair of constraints related to the reliability of the chemical composition measurement themselves), then the EPAR limit equals the PAR limit equals the MAR limit for that constraint. Finally, the DWPF control strategy has evolved over the course of radioactive operations. Revision 4 of this report introduced alternatives for satisfying some of the constraints as well as a new property-composition model for liquidus temperature. Revision 5 implemented several modifications to the acceptability decision at the DWPF that were recommended before the processing of Sludge Batch 4 (SB4). The modifications to PCCS, provided by this document, Revision 6, are necessary to be in place before SWPF becomes operational and becomes a contributor to the DWPF flowsheet.

4.0 Original Constraints for the Defense Waste Processing Facility (DWPF)

The original (at radioactive startup in 1996) constraints applicable to DWPF acceptability decisions are presented in Table 4-1, which provides the name of the constraint, the general form of the constraint, the type of constraint (i.e., what is the intended focus of the constraint), and the applicable uncertainties for the constraint. Note that no uncertainty is applied to the first constraint of Table 4-1, the conservation or “sum of oxides” constraint. The specification of this constraint was defined by the principal investigator of Reference 3 as a check on the reliability of the chemical composition measurements. The constraint is a bound on laboratory analyses based upon tolerable errors when attempting to predict durability from glass composition. As a result, no additional uncertainty need be incorporated when applying this constraint to the DWPF control strategy.

Table 4-1 Original Constraints Applicable to DWPF Process and Product Control

Name	Constraint	Type	Applicable Uncertainties
Conservation (sum of oxides)	95% ≤ Σ [Major Oxides in weight percent (wt%)] ≤ 105%	Laboratory Specification	None
Durability	B, Li, and Na Leach ≤ Environmental Assessment (EA) glass leach rate based upon Product Consistency Test [5]	Product Quality	Property and Measurement
Alumina	g Al_2O_3 / 100g glass ≥ 3.0	Product Quality	Measurement
Homogeneity	1.6035 sludge + 5.6478 frit > 216.8092 (Sludge and frit components, each as a wt%)	Product Quality	Measurement
Frit Loading	70% ≤ Σ (Frit Oxides in wt%) ≤ 85%	Product Quality	Measurement
Liquidus Temperature	Liquidus Temperature (T_L) ≤ 1050°C	Process-ability	Property and Measurement
Melt Viscosity at 1150°C	20 ≤ Viscosity (η) ≤ 100 poise (P)	Process-ability	Property and Measurement
TiO_2	g TiO_2 / 100g glass ≤ 1.0	Waste Solubility	Measurement
NaCl	g NaCl / 100g glass ≤ 1.0	Waste Solubility	Measurement
NaF	g NaF / 100g glass ≤ 1.0	Waste Solubility	Measurement
Cr_2O_3	g Cr_2O_3 / 100g glass ≤ 0.3	Waste Solubility	Measurement
SO_4 or Na_2SO_4	g SO_4 / 100g glass ≤ 0.40 g Na_2SO_4 / 100g glass ≤ 0.59	Waste Solubility	Measurement
Cu	g Cu / 100g glass ≤ 0.5	Waste Solubility	Measurement
PO_4 or P_2O_5	g PO_4 / 100g glass ≤ 3.0 g P_2O_5 / 100g glass ≤ 2.25	Waste Solubility	Measurement

Glass produced at the start of radioactive operations at the DWPF had to satisfy the constraints listed in Table 4-1 at the appropriate confidence levels. The confidence levels for the constraints associated with product acceptability or quality are discussed first. As detailed in the Waste Acceptance Product Specifications (WAPS) [4], the normalized boron, lithium, and sodium releases for DWPF glasses must be better than the corresponding releases for the Environmental Assessment (EA) glass based upon the Product Consistency Test (PCT) [5]. DWPF has chosen the option of showing that the PCT releases are at least "two sigma" better than the EA glass. This implies that these releases must be controlled to at least the 95% confidence level. Since the releases are predicted from durability-composition models, the property uncertainties associated with the models are determined to a 95% confidence in identifying the PARs and the MUs associated with the measured composition are determined to a 95% confidence in identifying the MAR. The other constraints identified in Table 4-1 as being related to product acceptability or quality do not involve property-composition models and as such only require that appropriate MU be applied. Once again, MUs are applied at the 95% confidence level for these constraints.

For the sake of consistency, the uncertainties (both property and measurement) of all other constraints (i.e., those associated with process-ability and solubility of waste components) are controlled to the same confidence level (i.e., 95%) in the discussion that follows. However, it is possible to adjust the confidence levels at which the other constraints are controlled at

management's discretion since they are non-waste-form-affecting (i.e., they are not associated with product acceptability or quality).

5.0 The Evolution of the Product Composition Control System (PCCS) Constraints

The purpose of this document, and of the PCCS that it supports, is and always has been the successful operation of the DWPF. As the DWPF radioactive processing progressed and associated studies at the Savannah River National Laboratory (SRNL) were completed, knowledge and experience were gained that offered solutions to problems and challenges that arose during the operation of that facility. Many of the SRNL efforts led to modifications to the constraints for successful DWPF operation. A goal of the revisions of this report has been to document this evolution of the original PCCS constraints provided in Table 4-1. To help meet that goal, this section provides a discussion of the impacts of SRNL studies supporting the SME acceptability process. This includes studies associated with the introduction of waste streams from SWPF into the DWPF flowsheet, which is the primary driver behind Revision 6 of this technical basis document.

5.1 Durability Model Applicability and Glass Homogeneity

One of the constraints of Table 4-1 associated with the durability of the DWPF waste form is the alumina constraint (i.e., $Al_2O_3 \geq 3$ wt%). When the durability models were developed, the B, Li, and Na releases for the original set of model glasses were reasonably well predicted by the durability models [3]. However, there appeared to be at least one separate population of glasses used for model development whose leach results were significantly under predicted. Most of these glasses were characterized by low concentrations of alumina. Therefore, the compositional region over which the durability models were to be applied was restricted to avoid production of low-alumina glasses.

Glass produced by the DWPF must be homogeneous for the first-principles, durability models utilized by PCCS to apply. To ensure homogeneous glass, the homogeneity constraint [6] that appears in Table 4-1 was included as part of the initial DWPF control strategy. This constraint was developed using glass information available at the time of the study, which led to a pair of additional constraints: the low and high frit loading constraints (Table 4-1). This pair of constraints was used to restrict glass compositions to a region for which the homogeneity constraint was deemed applicable [3].

As part of the glass variability study conducted by SRNL to support the processing of SB1b at the DWPF, it was determined that the homogeneity constraint would severely, and unnecessarily, limit the acceptable operating window for processing this sludge [7]. Based upon the results of that study, applying MU to the homogeneity constraint for SB1b was seen as overly conservative. It was determined from a preponderance of available data that the measurement acceptance requirement for the homogeneity constraint could be relaxed for SB1b as long as [7]:

- the Al_2O_3 concentration was greater than or equal to 4 wt% in the glass, or
- $Al_2O_3 \geq 3.0$ wt% and the sum of alkali, defined as $Cs_2O+K_2O+Li_2O+Na_2O$, in the glass was less than or equal to 19.3 wt%.

The implementation of either of the two options would require, however, application of the appropriate MUs (e.g., the $Al_2O_3 \geq$ [4.0 wt% + MU]). Also, note that the second option required monitoring of the alkali content in the SME samples, and thus introduced a new constraint that was implemented as part of Revision 4 of this document:

Equation 1 $Cs_2O + K_2O + Li_2O + Na_2O \leq 19.3$ wt%

SRNL conducted an evaluation of the lower limit of the frit loading constraint [8] and concluded that this constraint could be eliminated as long as the Al_2O_3 concentration in the glass was greater than or equal to 4.43 wt% plus MU. Additional SRNL studies that influenced how the question of homogeneity was addressed are discussed in Section 5.4.

5.2 Modification to Upper Limit for Viscosity Constraint

A re-evaluation of the viscosity constraints, conducted by SRNL [9] during the processing of SB1b, expanded the upper limit to 110 poise (P).

5.3 Modifications to Solubility Constraints

The solubility constraints of Table 4-1 have been modified in some cases as well. The solubility constraint associated with the P_2O_5 in the glass was removed from the scope of the PCCS as part of Revision 4 of this report and documented by an SRNL study [10]. Since the implementation of these changes in the PCCS, the P_2O_5 constraint has been handled administratively by the DWPF. As seen in Table 4-1, the 0.4 wt% solubility limit for SO_4 in glass is the original limit imposed in the PCCS. Before processing of SB3, SRNL conducted a study [11] that relaxed this limit to 0.6 wt% SO_4 in melter feed. No changes were made in PCCS to reflect the new limit, and the DWPF imposed the constraint on SO_4 solubility at the new limit administratively (outside of the formal PCCS). Similar SO_4 solubility studies have been and are expected to be conducted for each new sludge batch to determine an appropriate limit for SO_4 solubility. At this time, each such SO_4 solubility limit, if above 0.4 wt%, is to be controlled administratively by the DWPF. The manner in which the TiO_2 concentrations are to be constrained is addressed in Section 5.5.

5.4 Reduction of Constraints

Additional studies were conducted by SRNL to more fully establish the use of the alumina or alkali constraints discussed in Section 5.1 as replacements for the family of constraints related to glass homogeneity (i.e., the homogeneity, low frit, and high frit constraints). These studies were identified as reduction of constraints (ROC) efforts, and they were successful in replacing the family of homogeneity constraints (in their entirety) for sludge-only operations [12] and for coupled operations with TiO_2 content in the glass up to 2 wt% [13].

A ROC study was also deemed necessary before the coupled operation of DWPF with SWPF since TiO_2 concentrations in the resulting glass waste form are anticipated to exceed 2 wt% [14]. The results of that study led to the following constraints (Figure 5-1, where MUs must be applied) that replace the family of homogeneity constraints in their entirety:

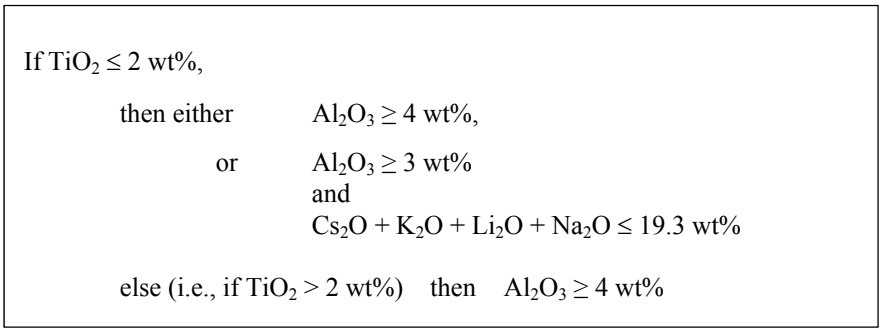

Figure 5-1 Reduction of Constraints for the DWPF Sludge-Only and Coupled with the Salt Waste Processing Facility (SWPF)

For situations with $TiO_2 \leq 2$ wt%, the alumina and alkali constraints described in Section 5.1 above are utilized. As seen in Figure 5-1, for situations with the TiO_2 content above 2 wt% in the glass, the Al_2O_3 content of the glass must be at or greater than 4 wt%. Note that MUs are to be applied in meeting the constraints indicated in this figure.

5.5 TiO_2 Constraint

A modification to the solubility constraint for TiO_2 was introduced as part of the changes of Revision 5. In Table 4-1, the limit on TiO_2 was set at 1.0 wt% based upon Reference 15. A subsequent study [16] relaxed the limit for TiO_2 to 2 wt%. The efforts associated with support for the introduction of waste streams from SWPF into the DWPF flowsheet involved the study of glass systems at higher concentrations of TiO_2, specifically, employing the glass test matrix defined in Reference 17. The results from that study led to the revision of the viscosity model [18], the durability models [14], and the liquidus temperature model [19] (these new models are discussed below). As a consequence of these results, the acceptability of DWPF's glass waste form at higher concentrations of TiO_2 is to be determined by the acceptability of the model predictions for viscosity, durability, and liquidus temperature. Thus, there is no longer a need for an individual solubility limit for TiO_2 in the DWPF glass waste form based upon the concentrations of TiO_2 expected during SWPF/DWPF coupled operations. However, there is a need to establish an upper model applicability limit on the TiO_2 concentration due to results from the viscosity modeling efforts for the higher TiO_2 glasses.

Results from several additional SRNL viscosity studies were investigated as part of the revision to the viscosity model [18], and these considered TiO_2 concentrations up to 8.38 wt%. These studies indicate that TiO_2 acts as a polymerizing agent and is tetrahedrally coordinated (4-coordinated) in waste glasses at these higher concentrations. The literature indicates that the switch in the role of TiO_2 from non-bridging oxide to a bridging oxide varies with the complexity of the overall glass composition. The exact TiO_2 concentrations at which TiO_2 switches from a network modifier to a network former lies somewhere between ~6.0 and 8.0 wt% TiO_2 for DWPF glass, and additional studies are needed to determine this limit more exactly. These higher TiO_2 studies were not evaluated in the viscosity modeling report. To avoid compositional regions where the role of TiO_2 in glass viscosity may change, an upper model applicability limit of 6.0 wt% on TiO_2 shall be utilized as part of the PCCS constraints.

Table 5-1 summarizes the constraints for SME acceptability determinations resulting from the changes discussed in Section 5.0 and adds the nepheline constraint which is discussed in Section 6.3.3.

Table 5-1 Satisfying Constraints Applicable to DWPF Process and Product Control

Name	Constraint at EPAR Limit	Comments
Low Conservation	95% ≤ Σ (Major Oxides in wt%)	No uncertainties need be applied to this constraint. Thus, the EPAR limit = PAR limit = MAR limit = 95% for this constraint.
High Conservation	Σ (Major Oxides in wt%) ≤ 105%	No uncertainties need be applied to this constraint. Thus, the EPAR limit = PAR limit = MAR limit = 105% for this constraint.
Durability	B, Li, and Na Leach ≤ EA glass Leach based upon PCT results	The EPAR limits and the active PAR and MAR uncertainties (at 95% confidence) for these constraints are discussed in Section 6.3.2. Compositions must satisfy the MAR for each of these constraints with 95% confidence.
Homogeneity	For TiO_2 ≤ (2 wt% - MU) Al_2O_3 ≥ (3.0 wt% + MU) and Σ alkali ≤ (19.3 wt% - MU) or Al_2O_3 ≥ (4.0 wt% + MU) For TiO_2 > (2 wt% - MU) Al_2O_3 ≥ (4.0 wt% + MU)	These constraints, expressed in wt% oxides, incorporate the alumina constraint as well as replace the original family of homogeneity constraints of Table 4-1 in their entirety. The impact of MU is indicated for these constraints.
Liquidus Temperature	Liquidus Temperature (T_L) ≤ 1050°C	There are active PAR and MAR uncertainties for this constraint that must be accounted for (these are discussed in Section 6.5). A composition must satisfy the MAR for this constraint (typically, with 95% confidence).
TiO_2	g TiO_2 / 100g glass ≤ (6.0 wt%- MU)	One of the changes introduced in this revision is the replacement of a solubility constraint by a viscosity modeling constraint where MU must be applied (typically, at a 95% confidence level).
Low Viscosity	20 poise (P) ≤ Viscosity (η) (with TiO_2 ≤ (6.0 wt%- MU) constraint met)	There are active PAR and MAR uncertainties for this constraint that must be accounted for (these are discussed in Section 6.4). A composition must satisfy the MAR for this constraint (typically, with 95% confidence).
High Viscosity	Viscosity (η) ≤ 110 poise (P) (with TiO_2 ≤ (6.0 wt%- MU) constraint met)	There are active PAR and MAR uncertainties for this constraint that must be accounted for (these are discussed in Section 6.4). A composition must satisfy the MAR for this constraint (typically, with 95% confidence).
NaCl[♣]	g NaCl / 100g glass ≤ 1.0	MU should be applied (typically, at a 95% confidence level) for this constraint; i.e., NaCl ≤ 1.0 - MU
NaF[♣]	g NaF / 100g glass ≤ 1.0	MU should be applied (typically, at a 95% confidence level) for this constraint; i.e., NaF ≤ 1.0 - MU
Cr_2O_3	g Cr_2O_3 / 100g glass ≤ 0.3	MU must be applied (typically, at a 95% confidence level) for this constraint; i.e., Cr_2O_3 ≤ 0.3 - MU
SO_4[♣] or Na_2SO_4	g SO_4 / 100g glass ≤ 0.40 g Na_2SO_4 / 100g glass ≤ 0.59	MU should be applied (typically, at a 95% confidence level) for this constraint; i.e., SO_4 ≤ 0.40 – MU. However, note that a SO_4 solubility study is frequently conducted for an individual sludge batch to provide a limited administrative modification to this constraint.
Cu	g Cu / 100g glass ≤ 0.5	MU must be applied (typically, at a 95% confidence level) for this constraint; i.e., Cu ≤ 0.5 - MU
Nepheline	$\frac{SiO_2}{SiO_2 + Na_2O + Al_2O_3} > 0.62$	The components of this formula are in mass fractions of the oxides in the glass, and glasses that satisfy this inequality do not tend to precipitate nepheline as their primary phase even under ccc heat treatment. MU must be applied to this constraint.

[♣] The uncertainty for each of these analytes was set to zero at the beginning of radioactive operations, and these values have not been modified as of yet.

6.0 Constraints and Uncertainties

The following subsections discuss the constraints listed in Table 5-1. Included in the discussion are the details of the uncertainties (both property and measurement, where appropriate) associated with meeting or satisfying each constraint at the desired confidence level. In general, the property model uncertainty must be computed for each constraint that involves a property-composition model. The computation depends on information generated during the fitting of the particular model, and this information is presented as part of the discussions for the sake of completeness. How this information is used in the computation of the property model uncertainty depends on the type of statistical interval selected to support the computation. Different types of statistical intervals are used depending on the situation. These issues are discussed in the subsections that follow.

The method for handling MU for each of the constraints is also discussed in the subsections that follow. Background information supporting these methods is presented as part of the discussion in Appendices A and B[f]. Also, in Appendix A, the complete set of chemical components used in PCCS is established as well as a single unit of measurement for handling the concentrations of these components. That unit of measure is molar oxide concentration (i.e., moles oxide per 100g glass), and the set of "average" molar oxide concentrations computed from a SME batch is represented by the row vector $\underline{z}$ (or $\underline{z}_n$ to indicate that the average is based on n samples).

To further simplify the assessment of the average SME composition against the acceptability constraints, the constraints will be transformed (to the extent possible) to an inequality of the form:

Equation 2

$$\underline{z}\,\underline{a}^T - \beta \geq 0$$

where $\underline{a}$ is a row vector of constants appropriate for the given constraint, β is the appropriate constraint offset (i.e., the remaining, non-composition-based term of the constraint inequality) for the given constraint, and $\underline{a}^T$ indicates the transpose of the $\underline{a}$ vector.

6.1 Conservation ("Sum of Oxides") Constraints

No uncertainties need to be applied to the conservation constraints. The specification for this pair of constraints was defined by the principal investigator of [3] as a check on the reliability of the chemical composition measurements themselves. They provide a bound on laboratory analyses based upon tolerable errors when attempting to predict durability from glass composition. As a result, no additional uncertainty need be incorporated when applying this pair of constraints to the DWPF control strategy. Thus, if the 95% and 105% limits are considered the EPAR limits, then the EPAR limits equal the PAR limits, which equal the MAR limits, for these constraints. Using the molar oxide notation to represent these constraints and letting M_{oxide} represent the molecular weight of the oxide yield♠:

[f] Appendices A and B are included in this revision for completeness. They have remained unchanged since Revision 3 of this report.

♠ The value utilized for the molecular weight of CuO in these conservation constraints is determined based upon the considerations presented in Section 7.1.

Equation 3 Low Sum of Oxides Constraint

$$z_{Al_2O_3} \cdot M_{Al_2O_3} + z_{B_2O_3} \cdot M_{B_2O_3} + z_{BaO} \cdot M_{BaO} + z_{CaO} \cdot M_{CaO} + z_{Ce_2O_3} \cdot M_{Ce_2O_3} + z_{Cr_2O_3} \cdot M_{Cr_2O_3}$$
$$+ z_{Cs_2O} \cdot M_{Cs_2O} + z_{CuO} \cdot M_{CuO} + z_{Fe_2O_3} \cdot M_{Fe_2O_3} + z_{K_2O} \cdot M_{K_2O} + z_{La_2O_3} \cdot M_{La_2O_3} + z_{Li_2O} \cdot M_{Li_2O}$$
$$+ z_{MgO} \cdot M_{MgO} + z_{MnO} \cdot M_{MnO} + z_{MoO_3} \cdot M_{MoO_3} + z_{Na_2O} \cdot M_{Na_2O} + z_{Nd_2O_3} \cdot M_{Nd_2O_3} + z_{NiO} \cdot M_{NiO}$$
$$+ z_{P_2O_5} \cdot M_{P_2O_5} + z_{PbO} \cdot M_{PbO} + z_{SiO_2} \cdot M_{SiO_2} + z_{ThO_2} \cdot M_{ThO_2} + z_{TiO_2} \cdot M_{TiO_2} + z_{U_3O_8} \cdot M_{U_3O_8}$$
$$+ z_{Y_2O_3} \cdot M_{Y_2O_3} + z_{ZnO} \cdot M_{ZnO} + z_{ZrO_2} \cdot M_{ZrO_2} - 95 \geq 0$$

Equation 4 High Sum of Oxides Constraint

$$z_{Al_2O_3} \cdot (-M_{Al_2O_3}) + z_{B_2O_3} \cdot (-M_{B_2O_3}) + z_{BaO} \cdot (-M_{BaO}) + z_{CaO} \cdot (-M_{CaO}) + z_{Ce_2O_3} \cdot (-M_{Ce_2O_3})$$
$$+ z_{Cr_2O_3} \cdot (-M_{Cr_2O_3}) + z_{Cs_2O} \cdot (-M_{Cs_2O}) + z_{CuO} \cdot (-M_{CuO}) + z_{Fe_2O_3} \cdot (-M_{Fe_2O_3}) + z_{K_2O} \cdot (-M_{K_2O})$$
$$+ z_{La_2O_3} \cdot (-M_{La_2O_3}) + z_{Li_2O} \cdot (-M_{Li_2O}) + z_{MgO} \cdot (-M_{MgO}) + z_{MnO} \cdot (-M_{MnO}) + z_{MoO_3} \cdot (-M_{MoO_3})$$
$$+ z_{Na_2O} \cdot (-M_{Na_2O}) + z_{Nd_2O_3} \cdot (-M_{Nd_2O_3}) + z_{NiO} \cdot (-M_{NiO}) + z_{P_2O_5} \cdot (-M_{P_2O_5}) + z_{PbO} \cdot (-M_{PbO})$$
$$+ z_{SiO_2} \cdot (-M_{SiO_2}) + z_{ThO_2} \cdot (-M_{ThO_2}) + z_{TiO_2} \cdot (-M_{TiO_2}) + z_{U_3O_8} \cdot (-M_{U_3O_8}) + z_{Y_2O_3} \cdot (-M_{Y_2O_3})$$
$$+ z_{ZnO} \cdot (-M_{ZnO}) + z_{ZrO_2} \cdot (-M_{ZrO_2}) - (-105) \geq 0$$

Note that the transformation of the constraints into a form similar to Equation 2 requires that the offset (the β) be expressed as a negative and that the $\underline{a}$ vector for the high "sum of oxides" constraint utilize the negatives of the molecular weights. Table 6-1 provides the complete information for these two constraints in the form of the vectors and offsets supporting Equation 2.

Table 6-1 Vectors and Offsets for the Sum of Oxide Constraints

	$\underline{z}^T$, Transpose of $\underline{z}$ vector		
	Average	Transpose of $\underline{a}$ Vectors	
	Molar Oxide		
Oxide	(moles oxide/100g glass)	$\underline{a}^T_{lowconsv}$	$\underline{a}^T_{highconsv}$
Al_2O_3	z_{Al2O3}	101.9612	-101.9612
B_2O_3	z_{B2O3}	69.6202	-69.6202
BaO	z_{BaO}	153.3394	-153.3394
HCOO	z_{HCOO}	0	0
CaO	z_{CaO}	56.0794	-56.0794
Ce_2O_3	z_{Ce2O3}	328.2382	-328.2382
NaCl	z_{NaCl}	0	0
Cr_2O_3	z_{Cr2O3}	151.9902	-151.9902
Cs_2O	z_{Cs2O}	281.8094	-281.8094
CuO	z_{CuO}	75.5439	-75.5439
NaF	z_{NaF}	0	0
Fe_2O_3	z_{Fe2O3}	159.6922	-159.6922
K_2O	z_{K2O}	94.2034	-94.2034
La_2O_3	z_{La2O3}	325.8182	-325.8182
Li_2O	z_{Li2O}	29.8774	-29.8774
MgO	z_{MgO}	40.3114	-40.3114
MnO	z_{MnO}	70.9374	-70.9374
MoO_3	z_{MoO3}	143.9382	-143.9382
NO_2	z_{NO2}	0	0
NO_3	z_{NO3}	0	0
Na_2O	z_{Na2O}	61.979	-61.979
Na_2SO_4	z_{Na2SO4}	0	0
Nd_2O_3	z_{Nd2O3}	336.4782	-336.4782
NiO	z_{NiO}	74.7094	-74.7094
P_2O_5	z_{P2O5}	141.9446	-141.9446
PbO	z_{PbO}	223.1894	-223.1894
SiO_2	z_{SiO2}	60.0848	-60.0848
ThO_2	z_{ThO2}	264.0368	-264.0368
TiO_2	z_{TiO2}	79.8988	-79.8988
U_3O_8	z_{U3O8}	842.0852	-842.0852
Y_2O_3	z_{Y2O3}	225.8082	-225.8082
ZnO	z_{ZnO}	81.3694	-81.3694
ZrO_2	z_{ZrO2}	123.2188	-123.2188
Offset (β)		95	-105
		$\beta_{low\ consv}$	$\beta_{high\ consv}$

Using the vectors of Table 6-1 to write these constraints for the sum of oxides in the form of Equation 2 yields:

Equation 5 Low Conservation: $\underline{z}\,\underline{a}^{\mathrm{T}}_{low\mathrm{consv}} - \beta_{low\mathrm{consv}} \geq 0$ or $\underline{z}\,\underline{a}^{\mathrm{T}}_{low\mathrm{consv}} - 95 \geq 0$

and

Equation 6 High Conservation:

$$\underline{z}\,\underline{a}^{T}_{highconsv} - \beta_{highconsv} \geq 0 \quad \text{or} \quad \underline{z}\,\underline{a}^{T}_{highconsv} - (-105) = \underline{z}\,\underline{a}^{T}_{highconsv} + 105 \geq 0$$

For a given average composition to be in the MAR (i.e., within the DWPF operating window), it must satisfy both of these "sum of oxide" constraints as given above.

6.2 Solubility Constraints and a TiO_2 Viscosity Model Constraint

As already mentioned the solubility constraint associated with P_2O_5 was removed from the scope of the PCCS control system as part of Revision 4 of this report [10], and the limit for TiO_2 solubility is replaced by a modeling limit based upon the results from the viscosity studies associated with the introduction of SWPF into the DWPF flowsheet [18]. In addition, as discussed above, an assessment of the TiO_2 content relative to a trigger value of 2 wt% must be determined as part of the evaluation of homogeneity for the SME batch (Figure 5-1) [14]; this is discussed in more detail in a following section.

Rewriting the solubility constraints of Table 5-1 using the molar oxide notation yields the following set of inequalities (the reference for each constraint is also indicated to the left of each of these inequalities):

Equation 7 NaCl Solubility [20] $z_{NaCl} M_{NaCl} \leq 1.0$

Equation 8 NaF Solubility [20] $z_{NaF} M_{NaF} \leq 1.0$

Equation 9 Cr_2O_3 Solubility [21] $z_{Cr_2O_3} M_{Cr_2O_3} \leq 0.3$

Equation 10 SO_4 Solubility [22] $\left\{ z_{SO_4} M_{SO_4} \leq 0.40 \quad \text{or} \quad z_{Na_2SO_4} M_{Na_2SO_4} \leq 0.59 \right\}$

Equation 11 Cu Solubility [23] $\left\{ z_{Cu} M_{Cu} \leq 0.5 \quad \text{or} \quad z_{CuO} M_{Cu} \leq 0.5 \right\}$

where $z_{Cu} \equiv z_{CuO}$

Equation 12 TiO_2 Model Limit [18] $z_{TiO_2} M_{TiO_2} \leq 6.0$

where, as before, M_{oxide} represents the molecular weight of the indicated oxide and z_{oxide} represents the "average" molar concentration (i.e., moles oxide/100g glass) for the indicated oxide.

Transforming these constraints to follow the form used in Equation 2 yields:

Equation 13 $z_{NaCl}(-M_{NaCl}) - (-1.0) \geq 0$

Equation 14 $z_{NaF}(-M_{NaF}) - (-1.0) \geq 0$

Equation 15 $z_{Cr_2O_3}(-M_{Cr_2O_3}) - (-0.3) \geq 0$

Equation 16 $z_{Na_2SO_4}(-M_{Na_2SO_4}) - (-0.59) \geq 0$

Equation 17 $z_{CuO}(-M_{Cu}) - (-0.5) \geq 0$

Equation 18 $$z_{TiO_2}\left(-M_{TiO_2}\right)-(-6.0)\geq 0$$

The shorthand notation when applied to these constraints yields an $\underline{a}$ vector with only a single "active" component (i.e., only one oxide of the vector $\underline{z}$ is involved in the constraint). Also, note in the Cu constraint, the multiplier is the molecular weight of elemental Cu, since the solubility constraint is a constraint on the elemental Cu in the waste form.

To complete the assessment of these constraints for a given composition requires that the appropriate uncertainties be accounted for in the constraints. Since no property-composition models are utilized in meeting the solubility constraints or in meeting the TiO_2 modeling constraint, no property model uncertainty need be applied. This leaves only MU for each of these constraints, and since each of the constraints involves a linear combination of the $\underline{z}$ vector of component concentrations, the MU can be addressed as described in Appendix B.

Using the approach of Appendix B, let $\underline{z}_n\underline{a}^T$ represent the linear combination of the average molar concentrations (based on n samples) of any one of these constraints and β represent the corresponding offset (Table 6-2 provides a complete listing of the vectors and offsets for these solubility constraints); then the constraint with MU would be of the form:

Equation 19 $$\underline{z}_n\underline{a}^T-\beta-t_\alpha(m-1)\sqrt{\frac{\underline{a}\mathbf{S}\underline{a}^T}{n}}\geq 0$$

where $t_\alpha(m\text{-}1)$ represents the upper 100 α% tail of the Student's t distribution with $m\text{-}1$ degrees of freedom and

Equation 20 $$\frac{\underline{a}\mathbf{S}\underline{a}^T}{n}\equiv \text{maximum}\left[\begin{array}{l}\dfrac{(\underline{a})\mathbf{S}_m(\underline{a})^T}{n}=\dfrac{1}{n}\displaystyle\sum_{j=0}^{q-1}\sum_{k=0}^{q-1}(\underline{a})_j(\underline{a})_k(\mathbf{S}_m)_{j,k}\\ \dfrac{(\underline{a})\mathbf{S}_n(\underline{a})^T}{n}=\dfrac{1}{n}\displaystyle\sum_{j=0}^{q-1}\sum_{k=0}^{q-1}(\underline{a})_j(\underline{a})_k(\mathbf{S}_n)_{j,k}\end{array}\right]$$

with S_m and S_n representing the covariance matrices (an absolute error structure based upon historical data versus a relative error structure based upon the current $\underline{z}$ vector, respectively) as described in Appendix B.

Table 6-2 Vectors and Offsets for Waste Solubility and TiO_2 Model Constraints

	$\underline{z}^T$	Transpose of $\underline{a}$ Vector for Each of the Solubility Constraints					
	Average						
	Molar Oxide						
Oxide	(moles oxide/100g glass)	$\underline{a}^T_{TiO2}$	$\underline{a}^T_{NaCl}$	$\underline{a}^T_{NaF}$	$\underline{a}^T_{Cr2O3}$	$\underline{a}^T_{Na2SO4}$	$\underline{a}^T_{Cu}$
Al_2O_3	z_{Al2O3}	0	0	0	0	0	0
B_2O_3	z_{B2O3}	0	0	0	0	0	0
BaO	z_{BaO}	0	0	0	0	0	0
HCOO	z_{HCOO}	0	0	0	0	0	0
CaO	z_{CaO}	0	0	0	0	0	0
Ce_2O_3	z_{Ce2O3}	0	0	0	0	0	0
NaCl	z_{NaCl}	0	-58.4428	0	0	0	0
Cr_2O_3	z_{Cr2O3}	0	0	0	-151.9902	0	0
Cs_2O	z_{Cs2O}	0	0	0	0	0	0
CuO	z_{CuO}	0	0	0	0	0	-63.5383
NaF	z_{NaF}	0	0	-41.9882	0	0	0
Fe_2O_3	z_{Fe2O3}	0	0	0	0	0	0
K_2O	z_{K2O}	0	0	0	0	0	0
La_2O_3	z_{La2O3}	0	0	0	0	0	0
Li_2O	z_{Li2O}	0	0	0	0	0	0
MgO	z_{MgO}	0	0	0	0	0	0
MnO	z_{MnO}	0	0	0	0	0	0
MoO_3	z_{MoO3}	0	0	0	0	0	0
NO_2	z_{NO2}	0	0	0	0	0	0
NO_3	z_{NO3}	0	0	0	0	0	0
Na_2O	z_{Na2O}	0	0	0	0	0	0
Na_2SO_4	z_{Na2SO4}	0	0	0	0	-142.0412	0
Nd_2O_3	z_{Nd2O3}	0	0	0	0	0	0
NiO	z_{NiO}	0	0	0	0	0	0
P_2O_5	z_{P2O5}	0	0	0	0	0	0
PbO	z_{PbO}	0	0	0	0	0	0
SiO_2	z_{SiO2}	0	0	0	0	0	0
ThO_2	z_{ThO2}	0	0	0	0	0	0
TiO_2	z_{TiO2}	-79.8988	0	0	0	0	0
U_3O_8	z_{U3O8}	0	0	0	0	0	0
Y_2O_3	z_{Y2O3}	0	0	0	0	0	0
ZnO	z_{ZnO}	0	0	0	0	0	0
ZrO_2	z_{ZrO2}	0	0	0	0	0	0
		-6.0	-1.0	-1.0	-0.30	-0.59	-0.50
	Offset (β)	β_{TiO2}	β_{NaCl}	β_{NaF}	β_{Cr2O3}	β_{Na2SO4}	β_{Cu}

This approach leads to the following expressions for the MAR associated with the solubility constraints.

Equation 21

$$\underline{z}_n \underline{a}^T_{NaCl} - (-1.0) - t_\alpha (m-1)\sqrt{\frac{\underline{a}_{NaCl}\mathbf{S}\,\underline{a}^T_{NaCl}}{n}} \geq 0$$

Equation 22

$$\underline{z}_n \underline{a}^T_{NaF} - (-1.0) - t_\alpha (m-1)\sqrt{\frac{\underline{a}_{NaF}\mathbf{S}\,\underline{a}^T_{NaF}}{n}} \geq 0$$

Equation 23
$$\underline{z}_n \underline{a}^T_{Cr_2O_3} - (-0.3) - t_\alpha (m-1)\sqrt{\frac{\underline{a}_{Cr_2O_3} \mathbf{S} \underline{a}^T_{Cr_2O_3}}{n}} \geq 0$$

Equation 24
$$\underline{z}_n \underline{a}^T_{Na_2SO_4} - (-0.59) - t_\alpha (m-1)\sqrt{\frac{\underline{a}_{Na_2SO_4} \mathbf{S} \underline{a}^T_{Na_2SO_4}}{n}} \geq 0$$

Equation 25
$$\underline{z}_n \underline{a}^T_{Cu} - (-0.5) - t_\alpha (m-1)\sqrt{\frac{\underline{a}_{Cu} \mathbf{S} \underline{a}^T_{Cu}}{n}} \geq 0$$

Equation 26
$$\underline{z}_n \underline{a}^T_{TiO_2} - (-6.0) - t_\alpha (m-1)\sqrt{\frac{\underline{a}_{TiO_2} \mathbf{S} \underline{a}^T_{TiO_2}}{n}} \geq 0$$

If all of these MAR constraints are satisfied, then $\underline{z}_n$ is acceptable for all of the waste solubility constraints and the TiO_2 modeling constraint. Note that the nominal 95% confidence level (equal to 100[1-α]%) for these constraints can be adjusted based upon management discretion.

6.3 Constraints Associated with Product Quality

Several of the constraints in Table 5-1 are associated with the quality of the DWPF waste form. For vitrified HLW, a quality product is a durable product, one that is resistant to leaching. The PCT [5], which yields normalized boron, lithium, and sodium releases, is used to assess waste glass durability. Since the durability of the DWPF glass product cannot be measured in situ, durability-composition models are used to predict the PCT response for the elements of interest. Such a model was developed for each of the three elements of interest (i.e., B, Li, and Na), and the form of these durability models may be represented as [3]:

Equation 27 Durability:‡
$$\log[NC_i] = m_d c_d + b_d$$
$$\text{where} \quad c_d \equiv \sum_{major\ oxides} z_{oxide} \Delta G_{oxide}$$

Constraints are derived from these models that restrict the DWPF glass compositions to those whose predicted PCT responses are "2-sigma" better than those of the EA glass. Figure 6-1 provides an illustration of these durability models. The fitted model (negatively sloped straight line) for boron is shown along with an upper (curved) 95% prediction limit. A cluster of points representing the EA glass PCT results for boron is indicated in the figure as well as a cluster of 5 points (circled) which led to the alumina constraint discussed above. More will be said in the discussions that follow regarding how the durability-composition models were used to develop and implement the durability constraints in PCCS. There were changes to this approach that were

‡ In general, this equation (with m_d being the estimated slope and b_d the estimated intercept) represents common logarithm (log) of the B, Li, and Na normalized releases, NC_i's, from the PCT. Specifically, c_d equals ΔG_p, the free energy of hydration (in kcal/mole) and thus uses all oxides described in Table IX of Ref. 3. A reasonable heuristic rule [4] is to use those oxides expected to be present in the DWPF glass product in appreciable amounts, i.e., ≥ 0.5 wt%. The individual coefficients for ΔG_p are obtained by pre-subtracting (as described in Ref. 3) the silica free energy, ΔG_{SiO_2}, from the free energy for each oxide expected to form a silicate, ΔG_{oxide}. The coefficient necessary for copper is defined uniquely in Section 7.1.

introduced as part of Revision 5 of this report, and the models themselves were modified slightly as a result of the studies to support the introduction of SWPF into the DWPF flowsheet [14].

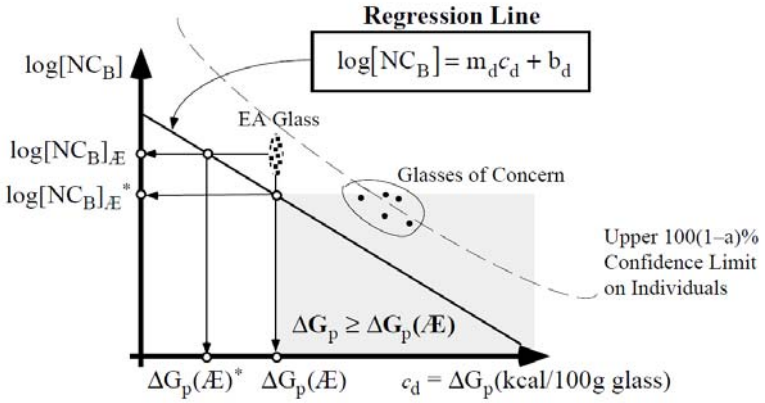

Figure 6-1 Product Consistency Test (PCT)-Based Durability Regression Line for Boron Release

As discussed in Sections 5.1 and 5.4, the glass must be homogeneous for the first-principles models as represented in Figure 6-1 to apply, and the constraints associated with homogeneity are represented in Figure 5-1.

DWPF complies with the WAPS [4] by showing that the normalized boron, lithium, and sodium releases for DWPF glasses are at least "2-sigma" less than the corresponding releases for the EA glass based upon the PCT leach test. This implies that these releases must be controlled to at least the 95% confidence level. Therefore, a 95% level of confidence is applied to all uncertainties (both property and measurement, where appropriate) associated with each of the constraints supporting the durability assessment including those evaluating homogeneity. These constraints are discussed in the subsections that follow.

6.3.1 Reduction of Constraints for Homogeneity

Four constraints in Table 5-1 that support the assessment of durability of the DWPF waste form are composition-only constraints. A fifth composition-only constraint, that supports the durability assessment, was introduced in Revision 5 of this report. It is a constraint that is associated with the formation of nepheline (a crystalline form that has the potential to introduce durability concerns), and it is addressed in the next section. These composition-only constraints do not rely on property-composition models; they can be most simply expressed in terms of mass oxide concentrations (i.e., x_{oxide} ≡ g oxide/100g glass). Expressing the interrelationships among these constraints in the form of "if-then-else" phrases yields:

If

Equation 28 $x_{TiO_2} \le 2.0$,

then

Equation 29 $x_{Al_2O_3} \ge 3.0$

and

Equation 30 Alkali: $x_{Cs_2O} + x_{K_2O} + x_{Li_2O} + x_{Na_2O} \le 19.3$ if $x_{Al_2O_3} < 4.0$

else

Equation 31 $x_{Al_2O_3} \geq 4.0$

Re-expressing these "if-then-else" phrases and the associated constraints in molar oxides yields:

If

Equation 32 $z_{TiO_2} M_{TiO_2} \leq 2.0$

then

Equation 33 $z_{Al_2O_3} M_{Al_2O_3} \geq 3.0$

and

Equation 34 $z_{Cs_2O} M_{Cs_2O} + z_{K_2O} M_{K_2O} + z_{Li_2O} M_{Li_2O} + z_{Na_2O} M_{Na_2O} \leq 19.3$

if $z_{Al_2O_3} M_{Al_2O_3} < 4.0$

or equivalently, if $z_{Al_2O_3} M_{Al_2O_3} \geq 4.0$ is not met

else

Equation 35 $z_{Al_2O_3} M_{Al_2O_3} \geq 4.0$

Using this same notation and transforming each of these constraints into a form similar to that provided in Equation 2, the "if-then-else" phases may be expressed as:

If

Equation 36 $z_{TiO_2}\left(-M_{TiO_2}\right)-\left(-2.0\right)\geq 0$

then

Equation 37 $z_{Al_2O_3} M_{Al_2O_3} - 3.0 \geq 0$

and

Equation 38

$$z_{Cs_2O}\left(-M_{Cs_2O}\right)+z_{K_2O}\left(-M_{K_2O}\right)+z_{Li_2O}\left(-M_{Li_2O}\right)+z_{Na_2O}\left(-M_{Na_2O}\right)-\left(-19.3\right)\geq 0$$

if $z_{Al_2O_3} M_{Al_2O_3} - 4.0 \geq 0$ is not met

else

Equation 39 $z_{Al_2O_3} M_{Al_2O_3} - 4.0 \geq 0$

As clarification, it should be noted that the constraint given by Equation 39 becomes limiting if Equation 36 is not met, and that Equation 38 becomes limiting if Equation 36 is met but Equation 39 is not met.

To complete the assessment of these constraints for a given composition requires that the appropriate uncertainties be accounted for in the constraints. Since no property-composition

models are utilized in meeting these constraints, no property model uncertainty need be applied. This leaves only MU for each of these constraints, and, since each of the constraints involves a linear combination of the $\underline{z}$ vector of component concentrations, the MU can be addressed as described in Appendix B.

Thus, letting $\underline{z}_n\underline{a}^T$ represent the linear combination of the average molar concentrations (based on n samples) of any one of these constraints and β the corresponding offset (Table 6-3 provides the vectors and offsets that allow these constraints to be placed in the form of Equation 2), then the constraint with MU would be of the form:

Equation 40

$$\underline{z}_n\underline{a}^T - \beta - t_\alpha(m-1)\sqrt{\frac{\underline{a}\mathbf{S}\underline{a}^T}{n}} \geq 0$$

where $t_\alpha(m\text{-}1)$ represents the upper 100 α% tail of the Student's t distribution with $m\text{-}1$ degrees of freedom and

Equation 41

$$\frac{\underline{a}\mathbf{S}\underline{a}^T}{n} \equiv \text{maximum}\left[\begin{array}{l} \dfrac{(\underline{a})\mathbf{S}_m(\underline{a})^T}{n} = \dfrac{1}{n}\displaystyle\sum_{j=0}^{q-1}\sum_{k=0}^{q-1}(\underline{a})_j(\underline{a})_k(\mathbf{S}_m)_{j,k} \\ \dfrac{(\underline{a})\mathbf{S}_n(\underline{a})^T}{n} = \dfrac{1}{n}\displaystyle\sum_{j=0}^{q-1}\sum_{k=0}^{q-1}(\underline{a})_j(\underline{a})_k(\mathbf{S}_n)_{j,k} \end{array}\right]$$

with S_m and S_n representing the covariance matrices (an absolute error structure based upon historical data versus a relative error structure based upon the current $\underline{z}$ vector, respectively) as described in Appendix B.

Table 6-3 Vectors and Offsets for TiO_2, Alumina, and Alkali Constraints

	$\underline{z}^T$	Transpose $\underline{a}$ Vector for Each of the Indicated Constraints			
	Average				
	Molar Oxide	with inter-relationships among these (see Figure 5-1)			
Oxide	(moles oxide/100g glass)	$\underline{a}^T_{TiO2}$	$\underline{a}^T_{Al2O3-1}$	$\underline{a}^T_{Al2O3-2}$	$\underline{a}^T_{alkali}$
Al_2O_3	z_{Al2O3}	0	101.9612	101.9612	0
B_2O_3	z_{B2O3}	0	0	0	0
BaO	z_{BaO}	0	0	0	0
HCOO	z_{HCOO}	0	0	0	0
CaO	z_{CaO}	0	0	0	0
Ce_2O_3	z_{Ce2O3}	0	0	0	0
NaCl	z_{NaCl}	0	0	0	0
Cr_2O_3	z_{Cr2O3}	0	0	0	0
Cs_2O	z_{Cs2O}	0	0	0	-281.8094
CuO	z_{CuO}	0	0	0	0
NaF	z_{NaF}	0	0	0	0
Fe_2O_3	z_{Fe2O3}	0	0	0	0
K_2O	z_{K2O}	0	0	0	-94.2034
La_2O_3	z_{La2O3}	0	0	0	0
Li_2O	z_{Li2O}	0	0	0	-29.8774
MgO	z_{MgO}	0	0	0	0
MnO	z_{MnO}	0	0	0	0
MoO_3	z_{MoO3}	0	0	0	0
NO_2	z_{NO2}	0	0	0	0
NO_3	z_{NO3}	0	0	0	0
Na_2O	z_{Na2O}	0	0	0	-61.979
Na_2SO_4	z_{Na2SO4}	0	0	0	0
Nd_2O_3	z_{Nd2O3}	0	0	0	0
NiO	z_{NiO}	0	0	0	0
P_2O_5	z_{P2O5}	0	0	0	0
PbO	z_{PbO}	0	0	0	0
SiO_2	z_{SiO2}	0	0	0	0
ThO_2	z_{ThO2}	0	0	0	0
TiO_2	z_{TiO2}	-79.8988	0	0	0
U_3O_8	z_{U3O8}	0	0	0	0
Y_2O_3	z_{Y2O3}	0	0	0	0
ZnO	z_{ZnO}	0	0	0	0
ZrO_2	z_{ZrO2}	0	0	0	0
	Offset (β)	-2	3	4	-19.3
		β_{TiO2}	$\beta_{Al2O3-1}$	$\beta_{Al2O3-2}$	β_{alkali}

This approach leads to the following expressions for the MAR associated with the implementation of these constraints.

If

Equation 42 $$\underline{z}_n \underline{a}^T_{TiO_2} - (-2) - t_\alpha (m-1)\sqrt{\frac{\underline{a}_{TiO_2} \mathbf{S}\, \underline{a}^T_{TiO_2}}{n}} \geq 0 \text{ is met}$$

then

Equation 43 $$\underline{z}_n \underline{a}^T_{Al_2O_3-1} - 3.0 - t_\alpha (m-1)\sqrt{\frac{\underline{a}_{Al_2O_3-1}\mathbf{S}\,\underline{a}^T_{Al_2O_3-1}}{n}} \geq 0$$ must be met

and

Equation 44 $$\underline{z}_n \underline{a}^T_{alkali} - (-19.3) - t_\alpha (m-1)\sqrt{\frac{\underline{a}_{alkali}\mathbf{S}\,\underline{a}^T_{alkali}}{n}} \geq 0$$ must be met

if $$\underline{z}_n \underline{a}^T_{Al_2O_3-2} - 4.0 - t_\alpha (m-1)\sqrt{\frac{\underline{a}_{Al_2O_3-2}\mathbf{S}\,\underline{a}^T_{Al_2O_3-2}}{n}} \geq 0$$ is not met

else

Equation 45 $$\underline{z}_n \underline{a}^T_{Al_2O_3-2} - 4.0 - t_\alpha (m-1)\sqrt{\frac{\underline{a}_{Al_2O_3-2}\mathbf{S}\,\underline{a}^T_{Al_2O_3-2}}{n}} \geq 0$$ must be met.

If these MAR constraints are appropriately satisfied, then $\underline{z}_n$ is acceptable for this set of ROC constraints that support the assessment of product quality for the SME batch. Thus, the options for satisfying these constraints detailed in this section are necessary to support the assessment of product quality and must be maintained at the 95% confidence level.

6.3.2 Durability Constraints

Glasses produced in the DWPF melter must have normalized releases for B, Li, and Na (as measured by the PCT) less than the corresponding releases for the EA glass. These releases cannot be routinely measured during DWPF operation; they instead have been related to glass composition (which can be measured) using simple regression models, as indicated above, of the form [3]:

Equation 46 $$\log[NC_i] = m_i \Delta G_p + b_i$$

where log represents the common logarithm,
i represents B, Li, or Na,
NC_i represents the normalized (PCT) release concentration in $g_{waste\ form}/L_{leachant}$ for element *i*,
m_i is the estimated slope of the simple linear regression for element *i*,
b_i is the estimated intercept of the simple linear regression for element *i*, and
ΔG_p represents the free energy of hydration (in kcal/mole), which is derived from the glass composition.

Reference 3 provides the complete background on the development of the durability-composition models that have been utilized as part of PCCS since the startup of radioactive operations. However, these models were re-evaluated as part of the studies associated with the integration of waste streams from SWPF into the DWPF flowsheet [14]. The result of that evaluation was the modification of these models to support a broader range of TiO_2 content [17]. Table 6-4 provides the regression information for each of the revised durability models. The estimated slope and intercept are provided along with the root mean square error (RMSE), s_i, associated with the fitted equation for each element, i. Some information common to all three models is also provided: the

sample size, n = 122, the number of estimated parameters, p = 2, and the X^TX matrix where X is determined from the vector of values associated with the independent variable, ΔG_p, which was used in the model fitting process.

Table 6-4 Regression Information Associated with Fitted Durability Models

i	m_i	b_i	RMSE, s_i	n=122	X^TX =	122	-1252.6109
B	-0.180215	-1.901602	0.195316			-1252.6109	13447.2741
Li	-0.145341	-1.541811	0.161483	p=2			
Na	-0.170473	-1.803846	0.168133				

The average normalized boron release for the EA glass is NC_B = 16.7 g/L or 1.2227 as a common logarithm. In DWPF, the intention is to control durability by controlling ΔG_p through the measured glass composition. The ΔG_p corresponding to the average EA glass boron release from the boron fitted model is:

Equation 47

$$\frac{\log[NC_B] - b_B}{m_B} = \Delta G_p \Rightarrow \frac{1.2227 - (-1.9016)}{-0.1802} = \Delta G_p = -17.3380$$

However, the ΔG_p computed from the measured chemical composition of the EA glass is –15.5186, which is considerably greater than the value derived from the regression line for boron release. Based upon the durability models (Figure 6-1), glass compositions with larger values of ΔG_p's are predicted to leach less (to be more durable) than glass compositions with smaller (more negative) ΔG_p's. Therefore, to be conservative, the ΔG_p value computed from the measured EA glass composition was used for the durability composition limit in initial versions of this report. One of the changes implemented in Revision 5 was the introduction of a less conservative approach to defining the durability composition limit. The details of this modified approach were provided in Reference 24. The results of this approach as applied to the revised models are summarized in the discussion below.

As stated above, the reference point for the durability comparisons is provided by the PCT results for samples of the EA glass. A series of PCTs (42 replicate durability assessments) was conducted on the EA glass with the results, which included the descriptive statistics provided in Table 6-5, reported in Reference 25.

Table 6-5 PCT Measurements Generated for the EA Standard Glass

Descriptor	B (g/L)	Li (g/L)	Na (g/L)
n (the number of PCTs conducted)	42	42	42
Mean	16.695	9.565	13.346
Standard Deviation (s)	1.222	0.735	0.902
Mean - 2×s	14.251	8.095	11.542

Table 6-5 provides the average of the normalized PCT responses for B, Li, and Na as well as the standard deviations of these responses. For reference, the value of the mean minus 2 times the

standard deviation is provided for each of the three elements as well. Note that the standard deviation used in this calculation is not the standard error of the sample mean (i.e., the standard deviation of the sample of PCTs divided by the square root of the sample size) but the sample standard deviation itself.

To meet the WAPS [4], DWPF must utilize an approach in PCCS that assures with high confidence that the mean PCT response for a DWPF waste form is less than the mean PCT response for EA (i.e., the glass making up the waste form is more durable than EA). Thus, using the available PCT measurements for EA summarized in Table 6-5, it would be reasonable to bound the lower limit of the mean EA response using a multiple of the standard error of the sample mean ($s/\sqrt{n}$) rather than of the larger (by a factor equal to the $\sqrt{n}$) sample standard deviation (s). However, the more conservative approach of using the larger of the two statistics (s versus $s/\sqrt{n}$) to bound the mean EA response was utilized in Revision 5, which is continued in this revision. Thus, if the DWPF is controlled such that the mean PCT response for each of its waste forms is below the limits given in the last row of Table 6-5 (with sufficient confidence), then the specifications outlined in the WAPS regarding the durability of the waste form have been met. In the next two subsections, these limits are incorporated into the uncertainty associated with the revised durability models in defining the EPARs and the PARs of Equation 46 to establish new limits on the values of ΔG_p as part of Revision 6 of this report.

6.3.2.1 Expected Property Acceptance Region (EPAR) For Durability

Let $\pi_i=\log(NC_i)$ for i=B, Li, and Na. Then, the common logarithms of the Mean – 2s values from Table 6-5 may be written as $\pi_B = 1.1538$, $\pi_{Li} = 0.9082$, and $\pi_{Na} = 1.0623$. Using this information and the models provided in Table 6-4, the ΔG_p value corresponding to the "expected" boron durability model for $\pi_B = 1.1538$ is given by:

Equation 48
$$\frac{\log[NC_B]-b_B}{m_B}=\Delta G_p \Rightarrow \frac{1.1538-(-1.9016)}{-0.1802}=\Delta G_p=-16.9556$$

Similarly, the ΔG_p for Li is given by -16.8617, and the ΔG_p for Na is given by -16.8100.

Thus, initially (before accounting for any property model uncertainty or MU), the durability constraints on $\underline{z}_n$, the average measured SME composition, may be written in the standard form as:

Equation 49
$$\underline{z}_n \underline{a}^T_{boron} - (-16.9556) \geq 0$$

Equation 50
$$\underline{z}_n \underline{a}^T_{lithium} - (-16.8617) \geq 0$$

Equation 51
$$\underline{z}_n \underline{a}^T_{sodium} - (-16.8100) \geq 0$$

where the $\underline{a}$ vectors are provided in Table 6-6 and are all identical. This set of equations provides the EPARs for the durability models. These EPAR values were different in Revision 5 as compared to the values given in earlier versions of this report, and with this revision they also

have been revised. The PARs (the β's) for these constraints are also included as part of the information in Table 6-6. The offsets of Table 6-6 (i.e., the PARs for the durability models) incorporate the appropriate property model uncertainties, which are discussed next.

Table 6-6 Vectors and Offsets for B, Li, and Na Durability Constraints

	$\underline{z}^T$			
	Average	Transpose of $\underline{a}$ Vectors for the Durability Constraints		
	Molar Oxide			
Oxide	(moles oxide/100g glass)	$\underline{a}^T_{boron}$	$\underline{a}^T_{lithium}$	$\underline{a}^T_{sodium}$
Al_2O_3	z_{Al2O3}	37.68	37.68	37.68
B_2O_3	z_{B2O3}	-10.43	-10.43	-10.43
BaO	z_{BaO}	-23.18	-23.18	-23.18
HCOO	z_{HCOO}	0	0	0
CaO	z_{CaO}	-13.79	-13.79	-13.79
Ce_2O_3	z_{Ce2O3}	-44.99	-44.99	-44.99
NaCl	z_{NaCl}	0	0	0
Cr_2O_3	z_{Cr2O3}	11.95	11.95	11.95
Cs_2O	z_{Cs2O}	-80.38	-80.38	-80.38
CuO	z_{CuO}	-4.95485	-4.95485	-4.95485
NaF	z_{NaF}	0	0	0
Fe_2O_3	z_{Fe2O3}	14.56	14.56	14.56
K_2O	z_{K2O}	-76.41	-76.41	-76.41
La_2O_3	z_{La2O3}	-48.59	-48.59	-48.59
Li_2O	z_{Li2O}	-24.04	-24.04	-24.04
MgO	z_{MgO}	-6.57	-6.57	-6.57
MnO	z_{MnO}	-24.44	-24.44	-24.44
MoO_3	z_{MoO3}	16.46	16.46	16.46
NO_2	z_{NO2}	0	0	0
NO_3	z_{NO3}	0	0	0
Na_2O	z_{Na2O}	-53.09	-53.09	-53.09
Na_2SO_4	z_{Na2SO4}	0	0	0
Nd_2O_3	z_{Nd2O3}	-37.79	-37.79	-37.79
NiO	z_{NiO}	0.37	0.37	0.37
P_2O_5	z_{P2O5}	-26.55	-26.55	-26.55
PbO	z_{PbO}	21.05	21.05	21.05
SiO_2	z_{SiO2}	4.05	4.05	4.05
ThO_2	z_{ThO2}	19.23	19.23	19.23
TiO_2	z_{TiO2}	16.27	16.27	16.27
U_3O_8	z_{U3O8}	-23.77	-23.77	-23.77
Y_2O_3	z_{Y2O3}	-12.91	-12.91	-12.91
ZnO	z_{ZnO}	0.92	0.92	0.92
ZrO_2	z_{ZrO2}	17.49	17.49	17.49
	Offset (β)	-14.395	-14.248	-14.476
		β_{boron}	$\beta_{lithium}$	β_{sodium}

6.3.2.2 Property Acceptance Region (PAR) for Durability

As evidenced by low-alumina glasses ([3] and [14]), PCT releases predicted from the ΔG_p-based models may be significantly biased. Furthermore, the glasses used to develop the durability

models exhibit appreciable scatter in measured PCT responses for narrow ranges of ΔG_p — more than would be suggested solely by the PCT methodology [3]. This causes difficulty, since the use of a regression model for durability prediction dictates that 1) the error in ΔG_p is negligible relative to that in PCT response (i.e., log[NC_i]) and 2) the error in the resulting regression model comes from that in the measured PCT response. The first condition seems reasonable for the model glasses as these were either measured by Corning Engineering Laboratory Services (CELS) or bias corrected to CELS standards. However, the fact that the measured PCT responses are more scattered over narrow ranges of ΔG_p than would be suggested by the analytical method indicates that additional sources of error may be unaccounted for.

To provide more conservative durability limits to account for departure from straight-line behavior and unaccounted for additional sources of variation, a one-sided $100(1-\alpha_0)\%$ simultaneous tolerance limit (where $1-\alpha_0$ is the coverage fraction) with $100(1-\alpha)\%$ confidence for multiple predictions will be used to define limits for durability. This is the same approach as was used in previous revisions of this report. The tolerance limits bound $100(1-\alpha_0)\%$ of all PCT release predictions at a confidence of $100(1-\alpha)\%$ for each and every ΔG_p value as opposed to bounding just the *mean* PCT release for each and every ΔG_p value. The new durability limit, π_i, which is considerably wider than the corresponding confidence band on the mean PCT release, is defined as the *upper* simultaneous tolerance interval for element i and is given by [26]:

Equation 52

$$\pi_i = b_i + m_i\left(c_i^*\right) + s_i\left\{\sqrt{pF_\alpha(p,n-p)}\sqrt{\underline{c}_0\left(\mathbf{X}^T\mathbf{X}\right)^{-1}\underline{c}_0^{\,T}} + z_{1-\alpha_0}\sqrt{\frac{n-p}{\chi^2_{\alpha/2,n-p}}}\right\}$$

where

- π_i equals the limiting value of log(NC_i), with i equal to B, Li, or Na (i.e., $\pi_B = 1.1538$, $\pi_{Li} = 0.9082$, and $\pi_{Na} = 1.0623$)
- the estimated slope and intercept of the fitted model for element i are given by m_i and b_i, respectively, (these values are given in Table 6-4),
- s_i is the RMSE for the fitted model for element i (the value is given in Table 6-4),
- $F_\alpha(p,n-p)$ is the F statistic, which depends on n (i.e., the number of data points on which this p-parameter model is based) and the desired confidence level as represented by (1-α)100%,
- the inverse product-moment matrix is represented by $(\mathbf{X}^T\mathbf{X})^{-1}$ where the product moment matrix contains information describing the data for the independent variable used to generate the regression equation (this matrix is given in Table 6-4),
- $\underline{c}_0$ is the vector, [1 c_i*], containing the parameter, c_i* (which is the PAR value to be computed for element i),
- $z_{1-\alpha_0}$ represents the one-sided $100(1-\alpha_0)\%$ percentile point from the standard normal distribution representing the $1-\alpha_0$ fraction of the model predictions to be covered, and
- $\chi^2_{\alpha/2,n-p}$ represents the lower (i.e., $\alpha/2$) percentile point of the χ^2 distribution with ($n-p$) degrees of freedom.

Let $c_{i,j}$ equal the i,jth element of the inverse product-moment matrix, $\mathbf{c} = \left(\mathbf{X}^T\mathbf{X}\right)^{-1}$ ♣. Therefore, the appropriate (i.e., upper) one-sided tolerance interval for the predicted release for element i at a given c_i* would be given by:

Equation 53

$$\pi_i = b_i + m_i\left(c_i^*\right) + s_i\left\{\sqrt{pF_\alpha(p,n-p)}\sqrt{\begin{bmatrix}1 & c_i^*\end{bmatrix}\begin{bmatrix}c_{0,0} & c_{0,1}\\ c_{0,1} & c_{1,1}\end{bmatrix}\begin{bmatrix}1\\ c_i^*\end{bmatrix}} + z_{1-\alpha_0}\sqrt{\frac{n-p}{\chi^2_{\alpha/2,n-p}}}\right\}$$

$$\pi_i = \left(b_i + s_i z_{1-\alpha_0}\sqrt{\frac{n-p}{\chi^2_{\alpha/2,n-p}}}\right) + m_i\left(c_i^*\right) + s_i\sqrt{pF_\alpha(p,n-p)}\sqrt{c_{1,1}\left(c_i^*\right)^2 + 2c_{0,1}\left(c_i^*\right) + c_{0,0}}$$

Thus, at a given limit, π_i, one of the roots, c_i*, of the following quadratic equation:

Equation 54

$$A\left(c_i^*\right)^2 + B\left(c_i^*\right) + C = 0$$

where

$$A \equiv m_i^{\,2} - c_{1,1}\left[ps_i^2 F_\alpha(p,n-p)\right]$$

$$B \equiv -2\left\{m_i\left(\pi_i - b_i - s_i z_{1-\alpha_0}\sqrt{\frac{n-p}{\chi^2_{\alpha/2,n-p}}}\right) + c_{0,1}\left[ps_i^2 F_\alpha(p,n-p)\right]\right\}$$

$$C \equiv \left(\pi_i - b_i - s_i z_{1-\alpha_0}\sqrt{\frac{n-p}{\chi^2_{\alpha/2,n-p}}}\right)^2 - c_{0,0}\left[ps_i^2 F_\alpha(p,n-p)\right]$$

provides the necessary tolerance interval. In Revision 3 of this report, algorithms were provided for estimating the percentiles of the z, χ^2, and F statistics used in these determinations. In Revision 4, these algorithms were eliminated since there was no need to compute these statistics for general values of degrees of freedom or significance level. The values needed for these calculations are provided in Table 6-7. Also, given in Table 6-7, are the PAR limits (truncated to three decimal places) for the B, Li, and Na durability constraints derived by solving the above equations using the information provided in this section.

♣ Note $(X^TX)^{-1}$ is a symmetric matrix; thus $c_{0,1} = c_{1,0}$.

Table 6-7 Durability Statistics and Predictions where p=2 and n=122

$\alpha = \alpha_0 = 0.05$	Values Used in and Determined by the Calculations of this Section
$z_{1-\alpha_0}$	1.6449
$\chi^2_{\alpha/2,n-p}$	91.57264
$z_{1-\alpha_0}\sqrt{\frac{n-p}{\chi^2_{\alpha/2,n-p}}}$	1.8830
$F_\alpha(p, n-p)$	3.0718
π_B	log(14.251) = 1.1538
π_{Li}	log(8.095) = 0.9082
π_{Na}	log(11.542) = 1.0623
B ΔG_p @ PAR	-14.395 kcal/mole
NL(B) @ PAR	4.51 g/L
Li ΔG_p @ PAR	-14.248 kcal/mole
NL(Li) @ PAR	3.09 g/L
Na ΔG_p @ PAR	-14.476 kcal/mole
NL(Na) @ PAR	4.23 g/L

These PAR ΔG_p limits for the B, Li, and Na models account not only for the desired property bounds but also for the random uncertainty inherent to the predictions. Figure 6-2 provides a graphical view of this process for boron. This figure provides a comparison of the PAR values for the Revision 5 model which was based on 131 data points and for the revised boron model which was based upon 122 data points (with 9 data points failing the ROC criteria of Figure 5-1 having been excluded from the modeling effort). A complete discussion of the revised models and similar graphs for lithium and sodium are provided in Reference 24. As seen in Figure 6-2, the revised boron model is less restrictive than the Revision 5 model (i.e., its PAR value is more negative than that of the earlier boron model); this is true for the revised lithium and sodium models as well. Thus, the revised models expand the DWPF operating window relative to the durability constraints, and all previous SME batches processed at the DWPF which satisfied the PAR constraints for the Revision 5 models for durability would also satisfy the PAR constraints for the revised models. The ΔG_p values for B, Li, and Na in Table 6-7 define these PAR limits, and thus, the offsets, for their corresponding durability constraints. Therefore, these are the values that appear at the bottom of Table 6-6.

Figure 6-2 The Boron Durability PAR Definition using Tolerance Intervals: Revision 5 (131 pts) and Revision 6 (122 pts)

6.3.2.3 Measurement Acceptance Region (MAR) for Durability Models

To complete the assessment of the durability constraints for a given composition requires that the MUs be accounted for in the constraints. Since each of the durability constraints involves a linear combination of the $\underline{z}$ vector of component concentrations, the MU for all of the durability constraints can be addressed as described in Appendix B.

Thus, letting $\underline{z}_n\underline{a}^T$ represent the linear combination of the average molar concentrations (based on n samples) of any one of these constraints and β the corresponding offset (Table 6-6), then the constraint with MU would be of the form:

Equation 55

$$\underline{z}_n\underline{a}^T - \beta - t_\alpha(m-1)\sqrt{\frac{\underline{a}\mathbf{S}\underline{a}^T}{n}} \geq 0$$

where t_α(m-1) represents the upper 100 α% tail of the Student's t distribution with m-1 degrees of freedom and

Equation 56

$$\frac{\underline{a}\mathbf{S}\underline{a}^T}{n} \equiv \text{maximum}\left[\begin{array}{l}\dfrac{(\underline{a})\mathbf{S}_m(\underline{a})^T}{n} = \dfrac{1}{n}\displaystyle\sum_{j=0}^{q-1}\sum_{k=0}^{q-1}(\underline{a})_j(\underline{a})_k(\mathbf{S}_m)_{j,k} \\ \dfrac{(\underline{a})\mathbf{S}_n(\underline{a})^T}{n} = \dfrac{1}{n}\displaystyle\sum_{j=0}^{q-1}\sum_{k=0}^{q-1}(\underline{a})_j(\underline{a})_k(\mathbf{S}_n)_{j,k}\end{array}\right]$$

with S_m and S_n representing the covariance matrices (an absolute error structure based upon historical data versus a relative error structure based upon the current $\underline{z}$ vector, respectively) as described in Appendix B.

This approach leads to the following expressions for the MAR associated with each of these durability constraints.

Equation 57

$$\underline{z}_n\,\underline{a}^T_{\text{boron}} - (-14.395) - t_\alpha(m-1)\sqrt{\frac{\underline{a}_{\text{boron}}\mathbf{S}\,\underline{a}^T_{\text{boron}}}{n}} \geq 0$$

Equation 58

$$\underline{z}_n\,\underline{a}^T_{\text{lithium}} - (-14.248) - t_\alpha(m-1)\sqrt{\frac{\underline{a}_{\text{lithium}}\mathbf{S}\,\underline{a}^T_{\text{lithium}}}{n}} \geq 0$$

Equation 59

$$\underline{z}_n\,\underline{a}^T_{\text{sodium}} - (-14.476) - t_\alpha(m-1)\sqrt{\frac{\underline{a}_{\text{sodium}}\mathbf{S}\,\underline{a}^T_{\text{sodium}}}{n}} \geq 0$$

If all of these MAR constraints are satisfied, then $\underline{z}_n$ is acceptable for this set of constraints that support the assessment of product quality for the SME batch. Since the MU is the same for all three elements, the most restrictive of these MAR constraints is that for lithium with the largest PAR value of -14.248. If Equation 58 is satisfied, then the other two equations will also be satisfied.

6.3.3 Nepheline Constraint

The introduction of a nepheline constraint into PCCS and the SME acceptability process was a major part of Revision 5 of this report and was prompted by the unique nature of SB4's composition [27]. As projections for the composition of SB4 were explored by the Liquid Waste Organization (LWO) as part of their planning for that sludge batch for DWPF, there was little doubt that the projected aluminum content for some of the options was pushing the resulting glass systems into compositional regions not processed previously by DWPF. At the same time, the application of the research by Li et al. [28] to the projected compositions suggested that there was a potential for nepheline formation for some of the glasses in these regions. As a result of these insights, the SRNL frit development team initiated a phased-study ([29], [30], [31], and [32]) of the nepheline discriminator proposed by Li et al. [28]. The results from these studies led to the team making the recommendation for the implementation of a nepheline constraint in PCCS before the processing of SB4 [27].

The high-alumina content of SB4, coupled with sodium contributions from both the sludge and frit, made the formation of a nepheline primary crystalline phase a potential problem for SB4 glass systems as waste loading was increased over the interval from 25 to 60%. While the problem was only seen in the centerline canister cooled (ccc) [33] version of study glasses, the nepheline discriminator was found to be a reliable aid in identifying glass compositions that are likely to form this primary crystalline phase under the ccc heat treatment [27]. The constraint is given by [28]:

Equation 60
$$\frac{SiO_2}{SiO_2 + Na_2O + Al_2O_3} > 0.62$$

where the chemical formula stands for the mass fractions of the oxides in the glass, and glasses that satisfy this inequality do not tend to precipitate nepheline as their primary phase even under ccc heat treatment.

Expressing Equation 60 in molar oxides and in the form of Equation 2 yields:

Equation 61
$$22.8322 \cdot SiO_2 - 38.4270 \cdot Na_2O - 63.2159 \cdot Al_2O_3 > 0$$

Note that the offset for the nepheline constraint as expressed in Equation 61 is 0. Table 6-8 provides the vector of coefficients ($\underline{a}^T$) and offset needed to represent the nepheline constraint.

To complete the assessment of the nepheline constraint for a given composition requires that the appropriate uncertainties be accounted for in the constraint. Given Equation 60 is an approximation to the nepheline primary phase field within the Al_2O_3-Na_2O-SiO_2 phase diagram [28], there was no statistical fitting of a model for this approximation. Therefore, no property model uncertainty need be applied. This leaves only MU for this constraint, which is addressed in the next section.

Table 6-8 Molar Oxide Vector and Offset for the Nepheline Constraint

	$\underline{z}^T$	
	Average	
	Molar Oxide	$\underline{a}^T$
Oxide	(moles oxide/100g glass)	Nepheline
Al_2O_3	z_{Al2O3}	-63.2159
B_2O_3	z_{B2O3}	0
BaO	z_{BaO}	0
HCOO	z_{HCOO}	0
CaO	z_{CaO}	0
Ce_2O_3	z_{Ce2O3}	0
NaCl	z_{NaCl}	0
Cr_2O_3	z_{Cr2O3}	0
Cs_2O	z_{Cs2O}	0
CuO	z_{CuO}	0
NaF	z_{NaF}	0
Fe_2O_3	z_{Fe2O3}	0
K_2O	z_{K2O}	0
La_2O_3	z_{La2O3}	0
Li_2O	z_{Li2O}	0
MgO	z_{MgO}	0
MnO	z_{MnO}	0
MoO_3	z_{MoO3}	0
NO_2	z_{NO2}	0
NO_3	z_{NO3}	0
Na_2O	z_{Na2O}	-38.4270
Na_2SO_4	z_{Na2SO4}	0
Nd_2O_3	z_{Nd2O3}	0
NiO	z_{NiO}	0
P_2O_5	z_{P2O5}	0
PbO	z_{PbO}	0
SiO_2	z_{SiO2}	22.8322
ThO_2	z_{ThO2}	0
TiO_2	z_{TiO2}	0
U_3O_8	z_{U3O8}	0
Y_2O_3	z_{Y2O3}	0
ZnO	z_{ZnO}	0
ZrO_2	z_{ZrO2}	0
	Offset (β)	0

To complete the assessment of the nepheline constraint for a given composition requires that the MUs be accounted for in the constraint. Since the constraint involves a linear combination of the $\underline{z}$ vector of component concentrations, the MU can be addressed as described in Appendix B.

Thus, letting $\underline{z}_n\underline{a}^T$ represent the linear combination of the average molar concentrations (based on n samples) for this constraint and β the corresponding offset (Table 6-8), then the constraint with MU would be of the form:

Equation 62

$$\underline{z}_n\underline{a}^T - \beta - t_\alpha(m-1)\sqrt{\frac{\underline{a}\mathbf{S}\underline{a}^T}{n}} \geq 0$$

where $t_\alpha(m\text{-}1)$ represents the upper 100 α% tail of the Student's t distribution with $m\text{-}1$ degrees of freedom and

Equation 63

$$\frac{\underline{a}\mathbf{S}\underline{a}^T}{n} \equiv \text{maximum}\left[\begin{array}{l}\dfrac{(\underline{a})\mathbf{S}_m(\underline{a})^T}{n} = \dfrac{1}{n}\displaystyle\sum_{j=0}^{q-1}\sum_{k=0}^{q-1}(\underline{a})_j(\underline{a})_k(\mathbf{S}_m)_{j,k} \\ \dfrac{(\underline{a})\mathbf{S}_n(\underline{a})^T}{n} = \dfrac{1}{n}\displaystyle\sum_{j=0}^{q-1}\sum_{k=0}^{q-1}(\underline{a})_j(\underline{a})_k(\mathbf{S}_n)_{j,k}\end{array}\right]$$

with S_m and S_n representing the covariance matrices (an absolute error structure based upon historical data versus a relative error structure based upon the current $\underline{z}$ vector, respectively) as described in Appendix B.

This approach leads to the following expressions for the MAR associated with the nepheline constraint.

Equation 64

$$\underline{z}_n\underline{a}^T_{nepheline} - t_\alpha(m-1)\sqrt{\frac{\underline{a}_{nepheline}\mathbf{S}\,\underline{a}^T_{nepheline}}{n}} \geq 0$$

If this MAR constraint is satisfied at the 95% confidence level, then $\underline{z}_n$ is acceptable for the nepheline constraint that supports the assessment of product quality for the SME batch.

6.4 Viscosity Constraints

A processing characteristic that is critical during DWPF melter operation is the viscosity of the melt. Once again, there is no opportunity for an in situ measurement of viscosity during processing; this melt property is predicted from the chemical composition of the SME material. For Revision 5 of this report, a new viscosity model developed by Jantzen [34] was implemented into the PCCS and SME acceptability. As part of the studies associated with the introduction of waste streams from SWPF into the DWPF flowsheet, Jantzen et al. [18] revised the viscosity model to cover glasses with a broader range of TiO_2 concentrations (i.e., up to 6 wt% in glass). The revised viscosity-composition model [18] is of the same form as previous viscosity models, so it may be implemented in the same manner ([34] and [35]):

Equation 65 Viscosity:[††]

$$\log(\eta) = m_v c_v + b_v$$

where

η is viscosity in poise (P),

m_v is the estimated slope for this regression model (m_v = -1.711755)

b_v is the estimated intercept (b_v = 3.382603),

[††] Actually the viscosity prediction is a three-parameter model including an inverse temperature term [27]. However, this temperature is fixed at 1150°C for DWPF. This allows the viscosity model to be presented as a two-parameter model with the temperature-dependent term included in the pseudo-constant, b_V.

$$c_v \equiv \frac{2\left(z_{Fe_2O_3} - z_{Al_2O_3} + z_{Cs_2O} + z_{Li_2O} + z_{K_2O} + z_{Na_2O}\right) + z_{TiO_2} + z_{B_2O_3}}{z_{SiO_2}}, \text{ and}$$

z_{oxide} represents the indicated molar oxide concentration in the glass.

This model can be back-solved to translate the viscosity constraints into constraints on the compositional term, c_v, as given by:

Equation 66 High Viscosity:

$$\text{high viscosity} \equiv \eta_{hv} \le 110 \text{ poise} \quad \Rightarrow \quad c_{hv} \ge \left[\frac{\log(\eta_{hv}) - b_v}{m_v}\right]$$

Equation 67 Low Viscosity:

$$\text{low viscosity} \equiv \eta_{lv} \ge 20 \text{ poise} \quad \Rightarrow \quad c_{lv} \le \left[\frac{\log(\eta_{lv}) - b_v}{m_v}\right]$$

The above inequalities describe the region in compositional space where all of the predicted values for viscosity are acceptable. This region defines the EPAR for viscosity. The region is denoted as "expected" since it is derived from the fitted line, which is the expected viscosity, based upon the model for a given composition.

6.4.1 Property Acceptance Region (PAR) for Viscosity

The determination of the PAR for the new viscosity model is accomplished by accounting for the property model uncertainty in the implementation of the viscosity constraints as was performed in earlier versions of this report for the previous viscosity models. And as before, statistical confidence intervals are used in the determinations of this uncertainty. Specifically, Scheffé simultaneous confidence limits (also called confidence bands [36] and [37]), are used in developing the PAR constraints associated with the revised viscosity model as they were for the previous models.

Since the revised viscosity model is of the same form as the previous models, it too includes a linear parameter based upon the inverse temperature (1/T) at which the viscosity (η) is measured. The complete form of the revised viscosity model may be expressed as:

Equation 68
$$\log(\eta) = m_v c_v + m_T \frac{1}{T(^\circ C)} + b_T$$

As indicated in an earlier footnote, for DWPF use, the temperature is fixed at 1150°C. Thus, the predicting relationship for viscosity can be written as:

Equation 69
$$\log(\eta) = m_v c_v + b_v$$

where $b_v \equiv \frac{m_T}{T(^\circ C)} + b_T$ and T(°C) is 1150°C.

However, the additional parameter must be accounted for when defining the confidence limits for viscosity prediction. In Revision 3 of this report, the approach used to develop the viscosity PAR was a conservative one that depended on two-sided, 100(1–α)% Scheffé-type confidence bands. Since each of the viscosity constraints is considered individually, the confidence level provided by this approach for each constraint is actually 100(1–α/2)%. In Revision 4 of this report the extra conservatism was no longer deemed necessary and the true one-sided, 100(1–α)% Scheffé-type confidence limit was used to determine the viscosity PAR. The same approach was used for the viscosity model introduced in Revision 5; and it is to be used for the revised model utilized in this revision. This leads to the following one-sided, 100(1–α)% Scheffé-type confidence limit to determine the PAR for each viscosity constraint:

Equation 70

$$\pi = b_T + \left(\frac{m_T}{T^*}\right) + m_v\left(c^*\right) + s_r\left\{\sqrt{pF_{2\alpha}(p,n-p)}\sqrt{\underline{c}_0\left(\mathbf{X}^T\mathbf{X}\right)^{-1}\underline{c}_0{}^T}\right\}$$

where π represents the EPAR for the corresponding constraint (20 P for low viscosity and 110 P for high viscosity), s_r is the RMSE in P for the regression fit, $F_{2\alpha}(p,n\text{-}p)$ is the upper 2α% tail of the F distribution with p degrees of freedom in the numerator and n-p degrees of freedom in the denominator, T^* = 1150ºC, c^* is the compositional term in Equation 65,

$$\underline{c}_0 \equiv \left[1, \frac{1}{T^*}, c^*\right] \text{ and } \mathbf{X} \equiv \begin{bmatrix} 1 & \frac{1}{T_1} & c_1 \\ 1 & \frac{1}{T_2} & c_2 \\ \vdots & \vdots & \vdots \\ 1 & \frac{1}{T_n} & c_n \end{bmatrix}.$$

X is an $n \times p$ matrix that contains the data for the independent variables from which the regression model was formulated where p is the number of parameters in the model and n is the number of observations used in the fitting of the new model. Note that the **X** matrix is different for the revised model (it includes measured compositions for additional glasses with higher TiO_2 content) as compared to the matrix that was used for the previous models. Thus, the product moment matrix, $\mathbf{X}^T\mathbf{X}$, for the revised model is different from that of the previous models but it is still of dimension 3x3 as for the previous models. The one-sided, 100(1–α)% Scheffé-type confidence limit to determine the PAR for each viscosity constraint may be written as:

Equation 71

$$\pi = b_T + \left(\frac{m_T}{T^*}\right) + m_v\left(c^*\right) + s_r\left\{\sqrt{pF_{2\alpha}(p,n-p)}\sqrt{\begin{bmatrix}1 & (1/T^*) & c^*\end{bmatrix}\begin{bmatrix} c_{0,0} & c_{0,1} & c_{0,2} \\ c_{0,1} & c_{1,1} & c_{1,2} \\ c_{0,2} & c_{1,2} & c_{2,2}\end{bmatrix}\begin{bmatrix}1 \\ (1/T^*) \\ c^*\end{bmatrix}}\right\},$$

where the inverse of the $\mathbf{X}^T\mathbf{X}$ matrix is represented by the 3×3 array of $c_{..}$'s. Since the (1/T*) term will be constant for DWPF use, the expression can be expanded for each viscosity constraint (i.e., low and high) to a quadratic in c* given by $A(c^*)^2 + B(c^*) + C = 0$ with coefficients given by the set of equations:

Equation 72

$$A \equiv m_v^{\,2} - c_{2,2}\left[ps_r^2 F_{2\alpha}(p, n-p)\right]$$

$$B \equiv -2\left\{m_v(\pi - b_T) + \left(c_{0,2} + \frac{c_{1,2}}{T^*}\right)\left[ps_r^2 F_{2\alpha}(p, n-p)\right]\right\}$$

$$C \equiv (\pi - b_T)^2 - \left[c_{0,0} + 2\left(\frac{c_{0,1}}{T^*}\right) + \frac{c_{1,1}}{(T^*)^2}\right]\left[ps_r^2 F_{2\alpha}(p, n-p)\right]$$

The information from the fitting of the new viscosity model [18] that is necessary to address its property uncertainty and, thus, to derive its PAR values is provided in Figure 6-3.

p = 3, n = 334, α = 0.05, m = -1.711755, b_T = 3.382603[1], s_r = 0.101351, and

$$\left(\mathbf{X}^T\mathbf{X}\right) = \begin{bmatrix} 334 & 0.299006 & 322.49187 \\ 0.299006 & 0.000270798 & 0.2899217 \\ 322.49187 & 0.2899217 & 319.71202 \end{bmatrix}$$

Figure 6-3 Information Generated from the Fitting of the Revised Viscosity Model

For the low viscosity constraint, the roots from the quadratic expression are 1.232996 and 1.200566, and selecting the desired root corresponding to the appropriate one-sided simultaneous confidence interval gives 1.200566 as the limit in composition space for the viscosity model, or

Equation 73 $$\eta = 10^{m_v c_v + b_v} = 10^{-1.711755 \times 1.200566 + 3.382603} = 10^{1.3275} = 21.26$$

(i.e., 21.26 poise at T* = 1150ºC). Only the SiO_2 coefficient in the low viscosity constraint is impacted; that is, the SiO_2 coefficient in the lower viscosity constraint vector is the root from the quadratic expression, or $\underline{a}_{\text{low visc},SiO_2}$ = 1.200566, while the coefficients of the other oxides are taken directly from their values in Equation 65. The complete $\underline{a}_{\text{low visc}}$ vector for the new viscosity model is provided in Table 6-9.

[1] The new melt viscosity model is a three parameter model [18] where the melt temperature is assumed to be 1150ºC, and thus the intercept provided is $b_v = b_T + (m_T/1150) = -0.606597 + (4587.5797/1150) = 3.382603$.

For the upper viscosity constraint the roots are 0.795480 and 0.770608. The desired root corresponding to the appropriate one-sided simultaneous confidence interval becomes 0.795480, or

Equation 74 $$\eta = 10^{m_v c_v + b_v} = 10^{-1.711755 \times 0.795480 + 3.382603} = 10^{2.02093} = 104.94$$

(i.e., 104.94 poise at T* = 1150ºC). Only the SiO_2 coefficient in the high viscosity constraint is impacted; that is, the SiO_2 coefficient in the high viscosity constraint vector is derived from the root from the quadratic expression, or $\underline{a}_{\text{high visc},SiO_2} = -0.795480$, while the coefficients of the other oxides are taken directly from their values in Equation 65. The complete $\underline{a}_{\text{high visc}}$ vector for the new viscosity model is provided in Table 6-9.

Table 6-9 Vectors and Offsets for the New Viscosity Constraints

	$\underline{z}^T$	Transpose of $\underline{a}$ Vectors for New Viscosity Constraints	
	Average Molar Oxide		
Oxide	(moles oxide/100g glass)	$\underline{a}^T_{\text{high visc}}$	$\underline{a}^T_{\text{low visc}}$
Al_2O_3	z_{Al2O3}	-2	2
B_2O_3	z_{B2O3}	1	-1
BaO	z_{BaO}	0	0
HCOO	z_{HCOO}	0	0
CaO	z_{CaO}	0	0
Ce_2O_3	z_{Ce2O3}	0	0
NaCl	z_{NaCl}	0	0
Cr_2O_3	z_{Cr2O3}	0	0
Cs_2O	z_{Cs2O}	2	-2
CuO	z_{CuO}	0	0
NaF	z_{NaF}	0	0
Fe_2O_3	z_{Fe2O3}	2	-2
K_2O	z_{K2O}	2	-2
La_2O_3	z_{La2O3}	0	0
Li_2O	z_{Li2O}	2	-2
MgO	z_{MgO}	0	0
MnO	z_{MnO}	0	0
MoO_3	z_{MoO3}	0	0
NO_2	z_{NO2}	0	0
NO_3	z_{NO3}	0	0
Na_2O	z_{Na2O}	2	-2
Na_2SO_4	z_{Na2SO4}	0	0
Nd_2O_3	z_{Nd2O3}	0	0
NiO	z_{NiO}	0	0
P_2O_5	z_{P2O5}	0	0
PbO	z_{PbO}	0	0
SiO_2	z_{SiO2}	-0.795480	1.200566
ThO_2	z_{ThO2}	0	0
TiO_2	z_{TiO2}	1	-1
U_3O_8	z_{U3O8}	0	0
Y_2O_3	z_{Y2O3}	0	0
ZnO	z_{ZnO}	0	0
ZrO_2	z_{ZrO2}	0	0
	Offset (β)	0	0
		$\beta_{\text{high visc}}$	$\beta_{\text{low visc}}$

6.4.2 Measurement Acceptance Region (MAR) for Viscosity

The MAR assessment of the revised viscosity model follows the same approach as was used for the previous viscosity models in earlier revisions of this report. Thus, completing the assessment of these constraints for a given composition requires that the MU for each of these constraints be accounted for. Since each of the viscosity constraints involves a linear combination of the $\underline{z}$ vector of component concentrations, the MU can be addressed as described in Appendix B.

Thus, letting $\underline{z}_n\underline{a}^T$ represent the linear combination of the average molar concentrations (based on n samples) of any one of these constraints and noting that the offsets (the β's) are zero for both constraints, then the constraint with MU would be of the form:

Equation 75

$$\underline{z}_n\underline{a}^T - t_\alpha(m-1)\sqrt{\frac{\underline{a}\mathbf{S}\underline{a}^T}{n}} \geq 0$$

where $t_\alpha(m\text{-}1)$ represents the upper 100 α% tail of the Student's t distribution with m-1 degrees of freedom and

Equation 76

$$\frac{\underline{a}\mathbf{S}\underline{a}^T}{n} \equiv \text{maximum}\left[\begin{array}{l}\dfrac{(\underline{a})\mathbf{S}_m(\underline{a})^T}{n} = \dfrac{1}{n}\displaystyle\sum_{j=0}^{q-1}\sum_{k=0}^{q-1}(\underline{a})_j(\underline{a})_k(\mathbf{S}_m)_{j,k} \\ \dfrac{(\underline{a})\mathbf{S}_n(\underline{a})^T}{n} = \dfrac{1}{n}\displaystyle\sum_{j=0}^{q-1}\sum_{k=0}^{q-1}(\underline{a})_j(\underline{a})_k(\mathbf{S}_n)_{j,k}\end{array}\right]$$

with S_m and S_n representing the covariance matrices (an absolute error structure based upon historical data versus a relative error structure based upon the current $\underline{z}$ vector, respectively) as described in Appendix B.

This approach leads to the following expressions for the MAR associated with each of the viscosity constraints.

Equation 77

$$\underline{z}_n\underline{a}^T_{\text{low visc}} - t_\alpha(m-1)\sqrt{\frac{\underline{a}_{\text{low vsic}}\mathbf{S}\,\underline{a}^T_{\text{low visc}}}{n}} \geq 0$$

Equation 78

$$\underline{z}_n\underline{a}^T_{\text{high visc}} - t_\alpha(m-1)\sqrt{\frac{\underline{a}_{\text{high visc}}\mathbf{S}\,\underline{a}^T_{\text{high visc}}}{n}} \geq 0$$

If this pair of MAR constraints is satisfied, then the SME composition, $\underline{z}_n$, is acceptable for each of the viscosity constraints at the (1-α)100% confidence level. It should be noted that the nominal 95% confidence level (equal to 100[1-α]%) for these constraints can be adjusted based upon management discretion.

6.5 Liquidus Temperature (T_L) Constraint

The liquidus temperature (T_L) for a glass is the *maximum* temperature at which the molten glass and primary crystalline phase (e.g., spinel for DWPF) are at equilibrium. The constraint on

liquidus temperature in the DWPF melter prevents melt pool crystallization during routine operation. This type of crystallization can involve almost simultaneous nucleation of the entire melt pool volume. When a significant amount of volume crystallization has occurred and the material has settled to the bottom of the melter, the pour spout may become partially or completely blocked. In addition, the melt pool may no longer be able to sustain Joule heating which would cause the melt pool to solidify. Finally, minimizing volume crystallization simultaneously minimizes subsequent devitrification of the glass once it is poured into a canister. Thus, even though the T_L constraint is non-waste-affecting, it still imposes an important limitation on the process-ability of a SME batch.

Glasses produced in DWPF must have liquidus temperatures below 1050ºC; this EPAR limit was defined to be safely below the nominal DWPF melter operating temperature of 1150ºC [18]. However, the liquidus temperature of a glass cannot be measured in situ, and consequently, T_L-composition models have been pursued. Incorporating a newly developed T_L model [38] into the SME acceptability decision and control system was one of the factors that motivated Revision 4 of this report. As part of the studies associated with the introduction of waste streams from SWPF into the DWPF flowsheet, Reference 19 revised the liquidus temperature model to cover glasses with a broader range of TiO_2 content (i.e., up to 6 wt% in glass). The revision to the model involved more than just a refitting of the coefficients of the previous model provided in Reference 38 to the broader glass compositional region; the required modifications are discussed below.

The approach in developing the T_L-composition model introduced in Revision 4 of this report employed a four-parameter model [38], which took the form:

Equation 79
$$\frac{1}{T_L(K)} = \ln\left\{(M_2)^a (M_1)^b (M_T)^c\right\} + d = a\ln(M_2) + b\ln(M_1) + c\ln(M_T) + d$$

or

Equation 80
$$T_L(^oC) = \left\{a\ln(M_2) + b\ln(M_1) + c\ln(M_T) + d\right\}^{-1} - 273$$

where K indicates temperature on the Kelvin scale,

$$\Sigma_{MT} \equiv \phi_{MT,SiO_2} z_{SiO_2} + \phi_{MT,Al_2O_3} z_{Al_2O_3} + \phi_{MT,Fe_2O_3} z_{Fe_2O_3}$$

$$\Sigma_{M1} \equiv \phi_{M1,Al_2O_3} z_{Al_2O_3} + \phi_{M1,Fe_2O_3} z_{Fe_2O_3} + \phi_{M1,TiO_2} z_{TiO_2} + \phi_{M1,Cr_2O_3} z_{Cr_2O_3} + \phi_{M1,ZrO_2} z_{ZrO_2} + \phi_{M1,NiO} z_{NiO} + \phi_{M1,MgO} z_{MgO} + \phi_{M1,MnO} z_{MnO}$$

$$\Sigma_{M2} \equiv \phi_{M2,NiO} z_{NiO} + \phi_{M2,MgO} z_{MgO} + \phi_{M2,MnO} z_{MnO} + \phi_{M2,CaO} z_{CaO} + \phi_{M2,K_2O} z_{K_2O} + \phi_{M2,Li_2O} z_{Li_2O} + \phi_{M2,Na_2O} z_{Na_2O}$$

$$\Sigma_{T1} \equiv \phi_{T1,SiO_2} z_{SiO_2} + \phi_{T1,Al_2O_3} z_{Al_2O_3} + \phi_{T1,Fe_2O_3} z_{Fe_2O_3} + \phi_{T1,TiO_2} z_{TiO_2}$$

$$\Sigma_{N1} \equiv \phi_{N1,K_2O} z_{K_2O} + \phi_{N1,Li_2O} z_{Li_2O} + \phi_{N1,Na_2O} z_{Na_2O}$$

$$M_2 \equiv \frac{\Sigma_{M2}}{\Sigma}, M_1 \equiv \frac{\Sigma_{M1}}{\Sigma}, M_T \equiv \frac{\Sigma_{MT}}{\Sigma}, \text{and } \Sigma \equiv \Sigma_{M2} + \Sigma_{M1} + \Sigma_{MT} + \Sigma_{T1} + \Sigma_{N1}$$

The ϕ coefficients of Equation 80 indicate the distribution of the various species that are needed to complete the modeling process [38]. With these speciation values specified, the least-squares fitting process for Equation 79 was conducted, using the data available during the previous model development effort, to estimate the parameters a, b, c, and d [38].

Use of the same four-parameter model was pursued after the data for the glasses with higher TiO_2 content were added to the previous modeling data set and with the same speciation values being used. The least-squares fitting process for Equation 79 was repeated to determine updated estimates of the a, b, c, and d parameters. However, the resulting model was found to be inadequate, which made it necessary to revise the speciation values as part of the model revision process. Table 6-10 provides the updated speciation values, and the least-squares fitting process for Equation 79, covering the expanded glass compositional region, yielded the parameter estimates: a = –0.000353617, b = –0.000691213, c = –0.000389016, and d = –0.002023544 [19].

Table 6-10 Speciation (ϕ) Coefficients Utilized in the Revised T_L Model [19]

Speciation (ϕ)	M2	M1	MT	N1	T1	SUM
Al_2O_3	0	0.0607	0.9393	0	0	1
B_2O_3	0	0	0	0	0	0
BaO						
HCOO						
CaO	0.029	0	0	0	0	0.029
Ce_2O_3						
NaCl						
Cr_2O_3	0	0.9202	0	0	0	0.9202
Cs_2O						
CuO						
NaF						
Fe_2O_3	0	0.127347	0.223553	0	0.503634	0.854534
K_2O	0.3041	0	0	0.1049	0	0.409
La_2O_3						
Li_2O	0.140267	0	0	0.064189	0	0.204456
MgO	0.0167	0.0223	0	0	0	0.039
MnO	0.994	0.006	0	0	0	1
MoO_3						
NO_2						
NO_3						
Na_2O	0.077275	0	0	0.136697	0	0.213972
Na_2SO_4						
Nd_2O_3						
NiO	0	0.1079	0	0	0	0.1079
P_2O_5						
PbO						
SiO_2	0	0	0.0193	0	0.0133	0.0326
ThO_2						
TiO_2	0	0.047186	0	0	0.148511	0.195697
U_3O_8						
Y_2O_3						
ZnO						
ZrO_2	0	0.0458	0	0	0	0.0458

As in the case for the earlier T_L-composition model introduced in Revision 4 of this report, the complexity of the revised model precludes its being re-stated as a linear combination of the average molar oxide concentration (i.e., following the format of Equation 2). This leads to PAR and MAR determinations that are unique to the T_L constraint ([38] and [19]).

6.5.1 Property Acceptance Region (PAR) for T_L

The determination of the T_L PAR is accomplished by accounting for the property model uncertainty for the revised T_L model and the approach is similar to that used for the viscosity constraints: a one-sided, 100(1−α)% Scheffé simultaneous lower confidence band on the inverse of liquidus temperature (or $1/T_L$) as given by:

Equation 81

$$\text{Prediction} - s_r\sqrt{pF_{2\alpha}(p,n-p)}\sqrt{\underline{c}_0\left(\mathbf{X}^T\mathbf{X}\right)^{-1}\underline{c}_0^{\,T}}$$

where s_r is the RMSE of the revised model, $F_{2\alpha}(p,n-p)$, is the 100(1−2α)% percentile of the F-distribution with p and n-p degrees of freedom in numerator and denominator, respectively, $\underline{c}_0$ is the vector of independent variables for which the prediction is to be made, and $(\mathbf{X}^T\mathbf{X})$ is the product moment matrix representing the independent variables used in fitting the model.

Because the inverse of liquidus temperature (or $1/T_L$) is predicted, the T_L constraint translates into a lower limit on $(1/T_L)$ of approximately $7.56\text{x}10^{-4}\text{K}^{-1}$. Therefore, the test for liquidus temperature should be one-sided based upon the one-sided lower bound on the $(1/T_L)$ prediction, or:

Equation 82

$$\frac{1}{T_L(K)} - s_r\sqrt{pF_{2\alpha}(p,n-p)}\sqrt{\underline{c}_0\left(\mathbf{X}^T\mathbf{X}\right)^{-1}\underline{c}_0^{\,T}} \geq 7.56x10^{-4}K^{-1}$$

where the predicted $(1/T_L)$ is obtained using the revised model above. Re-stating this constraint using information generated during the fitting of the model [19] leads to

Equation 83

$$\ln\left\{(M_2)^{-0.000353617}(M_1)^{-0.000691213}(M_T)^{-0.000389016}\right\} - 0.002023544$$
$$-\left(2.41717x10^{-5}\right)\sqrt{pF_{2\alpha}(p,N-p)}\sqrt{\xi\begin{bmatrix} 142 & -188.873614 & -388.925653 & -157.601204 \\ -188.873614 & 254.982966 & 515.389786 & 208.284252 \\ -388.925653 & 515.389786 & 1069.743318 & 428.191038 \\ -157.601204 & 208.284252 & 428.191038 & 181.683573 \end{bmatrix}^{-1}\xi^T}$$
$$\geq 7.56x10^{-4}K^{-1}$$

where ξ is defined to be the vector (i.e., [1 $\ln(M_2)$ $\ln(M_1)$ $\ln(M_T)$]) of values at which to predict $(1/T_L)$, p=4, and n=142, α=0.05 (or 5%), and thus, $F_{0.10}(4,138)=1.986045$. Thus, for a given SME composition, compute the values of $\ln(M_2)$, $\ln(M_1)$, and $\ln(M_T)$ and see whether this inequality is satisfied. If so, the composition is in the T_L PAR.

Another way of looking at the PAR for this constraint is to invert the PAR limit (after converting from Kelvin to the Celsius scale) for $1/T_L$ determined above, subtract away the predicted T_L derived from the model, and use this difference to represent the property prediction uncertainty. This amount can then be subtracted from the 1050°C EPAR limit to obtain the PAR limit in °C against which the T_L prediction can be directly compared. That is the predicted T_L has to be

below this PAR limit expressed in °C for the SME composition to be within the liquidus temperature PAR (with 95% confidence).

6.5.2 Measurement Acceptance Region (MAR) for T_L

In addition to the property uncertainty addressed in the previous section, any errors associated with measuring the SME composition from which the liquidus temperature is predicted must be introduced to assure that the glass in question will not crystallize in the DWPF melter. To estimate the relevant MUs for a given composition, the errors for the measured concentrations are first propagated through the model and the resulting variances and pair-wise covariances summed to provide an estimate of the measurement variance. Using this approach (as detailed in [38] and repeated in [19] for completeness), the estimated variance is given by:

Equation 84
$$V\left(\frac{1}{T_L}\right) \approx \sum_i \sum_j \left\{ \left[\frac{\partial}{\partial [i]} \left(\frac{1}{T_L}\right)_{pred} \right] (r_i [i]) \left[\frac{\partial}{\partial [j]} \left(\frac{1}{T_L}\right)_{pred} \right] (r_j [j]) \rho_{i,j} \right\}$$

for i and j from {Al_2O_3, CaO, Cr_2O_3, Fe_2O_3, K_2O, Li_2O, Na_2O, MgO, MnO, NiO, SiO_2, TiO_2, and ZrO_2} with

Equation 85
$$\left(\frac{1}{T_L}\right)_{pred} = \ln\left\{ (M_2)^{-0.000353617} (M_1)^{-0.000691213} (M_T)^{-0.000389016} \right\} - 0.002023544$$

where M_2, M_1, and M_T are defined in Equation 80.

In Equation 84, r_i, $[i]$, and $\rho_{i,j}$ are the relative standard deviation, molar concentration (on a 100g glass basis), and correlation coefficient of i and j, respectively. As in the determinations for the MARs for the other constraints, there are two options for representing the molar concentrations (i.e., the $[i]$'s): the historical average molar composition (computed using the historical average elemental composition of Table B2 in Appendix B) upon which the relative standard deviations (see Table B3 in Appendix B) and correlations (see Table B1 in Appendix B) were estimated and the average molar composition for the current SME batch, $\underline{z}_n$, based upon n samples. Once again, both representations will be considered with the larger MU from the two selected for use in the defining the T_L MAR.

The details of the estimation of the measurement variance are provided in References 38 and 19. Table 6-11 summarizes the critical information needed in evaluating the partial derivatives for each molar oxide of interest. In this table, the vector of partial derivatives (evaluated at the SME composition, $\underline{z}_n$) is represented by $\underline{p}$. These partial derivatives are provided as expressions of the model terms (sum, sm1, sm2, and smt), the model coefficients (a, b, c, and d), and the speciation values (labeled A through Y) for the model terms.

Table 6-11 Evaluation of Partial Derivatives at SME Average Molar Composition

	Evaluation of Partial Derivatives of Model				
	with respect to Individual Oxides				
Oxide	**— Vector of partials represented by $\underline{p}^T$ —**			**where**	
Al_2O_3	-((a+b+c)/sum)*AA+((H*b/sm1)+Q*c/smt)	sum	=	Σ	in T_L model
B_2O_3	0	sm1	=	M_1	in T_L model
BaO	0	sm2	=	M_2	in T_L model
HCOO	0	smt	=	M_T	in T_L model
CaO	-((a+b+c)/sum)*D+(D*a/sm2)	a	=	-0.000353617	in T_L model
Ce_2O_3	0	b	=	-0.000691213	in T_L model
NaCl	0	c	=	-0.000389016	in T_L model
Cr_2O_3	-((a+b+c)/sum)*K+(K*b/sm1)	d	=	-0.002023544	in T_L model
Cs_2O	0	A	=	0	NiO in ΣM2
CuO	0	B	=	0.0167	MgO in ΣM2
NaF	0	C	=	0.994	MnO in ΣM2
Fe_2O_3	-((a+b+c)/sum)*BB+((I*b/sm1)+R*c/smt)	D	=	0.029	CaO in ΣM2
K_2O	-((a+b+c)/sum)*CC+(E*a/sm2)	E	=	0.3041	K_2O in ΣM2
La_2O_3	0	F	=	0.140267	Li_2O in ΣM2
Li_2O	-((a+b+c)/sum)*DD+(F*a/sm2)	G	=	0.077275	Na_2O in ΣM2
MgO	-((a+b+c)/sum)*EE+(B*a/sm2)+(N*b/sm1)	H	=	0.0607	Al_2O_3 in ΣM1
MnO	-((a+b+c)/sum)*FF+(C*a/sm2)+(O*b/sm1)	I	=	0.127347	Fe_2O_3 in ΣM1
MoO_3	0	J	=	0.047186	TiO_2 in ΣM1
NO_2	0	K	=	0.9202	Cr_2O_3 in ΣM1
NO_3	0	L	=	0.0458	ZrO_2 in ΣM1
Na_2O	-((a+b+c)/sum)*GG+(G*a/sm2)	M	=	0.1079	NiO in ΣM1
Na_2SO_4	0	N	=	0.0223	MgO in ΣM1
Nd_2O_3	0	O	=	0.006	MnO in ΣM1
NiO	-((a+b+c)/sum)*HH+(A*a/sm2)+(M*b/sm1)	P	=	0.0193	SiO_2 in ΣMT
P_2O_5	0	Q	=	0.9393	Al_2O_3 in ΣMT
PbO	0	R	=	0.223553	Fe_2O_3 in ΣMT
SiO_2	-((a+b+c)/sum)*II+(P*c/smt)	S	=	0.1049	K_2O in ΣN1
ThO_2	0	T	=	0.064189	Li_2O in ΣN1
TiO_2	-((a+b+c)/sum)*JJ+(J*b/sm1)	U	=	0.136697	Na_2O in ΣN1
U_3O_8	0	V	=	0.0133	SiO_2 in ΣT1
Y_2O_3	0	W	=	0	Al_2O_3 in ΣT1
ZnO	0	X	=	0.503634	Fe_2O_3 in ΣT1
ZrO_2	-((a+b+c)/sum)*L+(L*b/sm1)	Y	=	0.148511	TiO_2 in ΣT1
		AA	=	W+H+Q	
		BB	=	X+I+R	
		CC	=	S+E	
		DD	=	F+T	
		EE	=	N+B	
		FF	=	C+O	
		GG	=	U+G	
		HH	=	A+M	
		II	=	P+V	
		JJ	=	Y+J	

As previously stated the MU is to be computed using both the historical and current SME compositions. These calculations are made relative to the PAR limit computed in the previous section. First, consider the MU derived using the current SME composition. Let the vector $\underline{r}$

represent the relative standard deviations of Table B3 and $\underline{C}_m$ represents the correlation matrix of Table B1, then compute the vector $\underline{s}_m$ by

Equation 86 $\underline{\mathbf{s}}_\mathbf{m} = (\underline{\mathbf{z}} \# \underline{\mathbf{r}} \# \underline{\mathbf{p}})$

where the operator # implies element by element multiplication between two vectors.

Next, compute S_m as

Equation 87 $S_m = \underline{s}_m * \underline{C}_m * \underline{s}_m'$

The final step in assessing the impact of MU using the current SME composition is to compute:

Equation 88 $$MAR_{current} = PAR_{1/T_L} + t_\alpha (m-1) \cdot \sqrt{S_m / n}$$

where PAR_{1/T_L} represents the PAR limit as $1/T_L$ (i.e., for the original model) and $t_\alpha(m\text{-}1)$ is the upper 100α % tail of the Student's t distribution with m-1 degrees of freedom.

A similar approach is used to estimate the MU derived using the historical composition. Let the vectors $\underline{g}$ and $\underline{M}$ represent the gravimetric factors and molecular weights, respectively, of Table A2 and the vector $\underline{h}$ represent the historical elemental compositions of Table B2, then compute the vector $\underline{s}_n$ by

Equation 89 $\underline{\mathbf{s}}_\mathbf{n} = (\underline{\mathbf{g}} \# \underline{\mathbf{h}} \# \underline{\mathbf{r}} \# \underline{\mathbf{p}})/\underline{\mathbf{M}}$

where once again, the operator # implies element by element multiplication between two vectors and the division represented by "/" is also element by element.

Next, compute S_n as

Equation 90 $S_n = \underline{s}_n * \underline{C}_m * \underline{s}_n'$

The final step in assessing the impact of MU using the historical composition is to compute:

Equation 91 $$MAR_{historical} = PAR_{1/T_L} + t_\alpha (m-1) \cdot \sqrt{S_n / n}$$

where PAR_{1/T_L} represents the PAR limit as $1/T_L$ (i.e., for the Equation 79 model) and $t_\alpha(m\text{-}1)$ is the upper 100α % tail of the Student's t distribution with m-1 degrees of freedom.

As the final step in assessing the MU for the liquidus temperature model, find the larger of $MAR_{historical}$ and $MAR_{current}$; call this value, MAR_{1/T_L}, since it is still in terms of $1/T_L$. This MAR limit may be expressed in °C as:

Equation 92 $$MAR_{T_L} = \left(1 / MAR_{1/T_L} \right) - 273$$

A SME composition with a predicted T_L value less than MAR_{T_L} would satisfy the liquidus temperature MAR with 95% confidence. Note that the nominal 95% confidence level (equal to $100[1\text{-}\alpha]\%$) for the T_L constraint can be adjusted based upon management discretion.

7.0 Reduction/Oxidation (REDOX) Considerations

The majority of elements considered in PCCS possess only a single corresponding oxide – they are assumed to be either completely oxidized or reduced at current DWPF melter conditions – as indicated by References 39 and 40. There are only two exceptions: iron and copper,[†] which are discussed in the following sections. DWPF currently measures the REDOX ratio for their SME feed; typically, a REDOX ratio of ~0.2 is targeted [41]. However, this ratio is assumed to be zero for current DWPF use (i.e., it is currently assumed that all Fe is converted to Fe_2O_3). This approach was taken based upon a REDOX study for SB2 which showed no evidence of a need for the activation of the REDOX term in PCCS [42]. How to activate a REDOX term in PCCS, if circumstances change and it becomes warranted, is addressed in Section 7.2.

Alternatively, the elemental copper will be approximately half reduced and half oxidized in the DWPF glass. This has an impact on both the durability and conservation constraint calculations.[††]

7.1 REDOX Issues for Copper (Cu)

The ratio of Cu^{1+} (reduced) to total copper (i.e., Cu^{1+} and Cu^{2+}) is assumed to be 0.5 based upon References 39 and 40. The concentrations of Cu_2O (reduced) and CuO (oxidized) are thus:

Equation 93

$$\phi_{Cu} \equiv \frac{g\,Cu^{1+}}{g\,Cu^{1+} + g\,Cu^{2+}} \text{ and } \frac{g\,Cu^{2+}}{g\,Cu^{1+} + g\,Cu^{2+}} = 1 - \phi_{Cu}$$

and

Equation 94

$$\underline{x}_{Cu} \equiv \frac{g\,Cu}{100g\ glass} = \frac{g\,Cu^{1+} + g\,Cu^{2+}}{100g\ glass}$$

or

Equation 95

$$\underline{z}_{Cu_2O} = \frac{\gamma_{Cu_2O}}{M_{Cu_2O}} \phi_{Cu}\, \underline{x}_{Cu}$$

and

Equation 96

$$\underline{z}_{CuO} = \frac{\gamma_{CuO}}{M_{CuO}} \left[1 - \phi_{Cu}\right] \underline{x}_{Cu},$$

where γ_i is the gravimetric factor converting from mass of elemental copper to mass of corresponding oxide, i.

[†] For DWPF use, elemental iron is properly assumed to be completely oxidized [39, 40]. Manganese is the only element that will be almost completely reduced in DWPF glasses; therefore, its corresponding oxide is MnO [40].

[††] This has no impact on the copper constraint, which is based on total elemental copper as is measured during DWPF processing.

For durability, the contribution to the total free energy of hydration for copper is:‡

Equation 97

$$\left(\Delta G_{Cu_2O} - \Delta G_{SiO_2}\right)\underline{z}_{Cu_2O} + \left(\Delta G_{CuO} - \Delta G_{SiO_2}\right)\underline{z}_{CuO}$$

where the copper ΔG_i coefficients are taken from Reference 3. It would be desirable to define an aggregate ΔG_i for copper, designated ΔG_{Cu_xO}, that would allow the copper free energy contribution to be estimated from the total elemental copper concentration if the copper is assumed to be completely oxidized (i.e., all Cu is converted to CuO). This would take the form:

Equation 98

$$\left(\Delta G_{Cu_xO} - \Delta G_{SiO_2}\right)\underline{z}_{All\ \mathrm{Cu\ as\ CuO}} \equiv \left(\Delta G_{Cu_2O} - \Delta G_{SiO_2}\right)\underline{z}_{Cu_2O} + \left(\Delta G_{CuO} - \Delta G_{SiO_2}\right)\underline{z}_{CuO}$$

The copper could then be managed in the same fashion as all other elements in the durability constraint computations (i.e., it would possess a single corresponding oxide). This aggregate ΔG_i coefficient is then:

Equation 99

$$\Delta G_{Cu_xO} \equiv \phi_{Cu}\left(\frac{\gamma_{Cu_2O}}{M_{Cu_2O}}\right)\left(\frac{M_{CuO}}{\gamma_{CuO}}\right)\left(\Delta G_{Cu_2O} - \Delta G_{SiO_2}\right) + \left(1-\phi_{Cu}\right)\left(\Delta G_{CuO} - \Delta G_{SiO_2}\right) + \Delta G_{SiO_2}$$

Similarly, the conservation of mass constraint is affected by the differing possible complexes of copper in the DWPF melt. The oxide contribution for copper should be:

Equation 100

$$\frac{g\ Cu_2O + g\ CuO}{100 g\ glass} \equiv \phi_{Cu}\gamma_{Cu_2O}\underline{x}_{Cu} + \left(1-\phi_{Cu}\right)\gamma_{CuO}\underline{x}_{Cu}$$

However, if all copper is assumed to be oxidized, the following contribution is actually made to the oxide sum due to copper:

Equation 101

$$\frac{g\ CuO}{100 g\ glass} \equiv \gamma_{CuO}\underline{x}_{Cu}$$

Therefore, the constraint coefficient for conservation must be multiplied by a factor of:

Equation 102

$$\frac{\phi_{Cu}\gamma_{Cu_2O} + \left(1-\phi_{Cu}\right)\gamma_{CuO}}{\gamma_{CuO}}$$

to assure that the correct contribution is made for copper. Thus all copper can be considered oxidized without invalidating any property constraints.

The assumptions and manipulations made concerning copper and its corresponding oxide form do not impact the variance estimates computed for acceptability testing. In DWPF only total copper will be measured; therefore, only the total elemental copper has a variance component associated

‡ Both copper ΔG_i coefficients have the free energy for silica subtracted from them since they both form silicates [3].

with it.† Using the above transformations, i.e., assuming the copper is oxidized, will provide the appropriate variance component for testing.

7.2 REDOX Issues for Iron (Fe)

As previously stated two cations (Cu and Fe) in PCCS are considered multivalent at expected DWPF operating conditions. That is, the Cu can be in either the I or II state (and is currently assumed to be a 50/50 split of the two) and the Fe can be in either the II or III state (and is currently considered to be entirely oxidized or in the III state). As illustrated in the previous section, this impacts two sets of constraints (i.e., those on durability and those on mass conservation). Because of the inherent imprecision of the REDOX determination, it is only desired to bound the potential impact of the multivalent cations on glass durability as described by the durability model predictions.

A derivation for Fe similar to that used for Cu in the previous section supplies the appropriate ΔG_p coefficient, $\Delta G_{Fe_xO_y}$, for Fe under more general REDOX conditions:

Equation 103

$$\Delta G_{Fe_xO_y} \equiv \phi_{Fe}\left(\frac{\gamma_{FeO}}{M_{FeO}}\right)\left(\frac{M_{Fe_2O_3}}{\gamma_{Fe_2O_3}}\right)\left(\Delta G_{FeO} - \Delta G_{SiO_x}\right) + \left(1-\phi_{Fe}\right)\Delta G_{Fe_2O_3}$$

where ϕ_{Fe} is the fraction of iron in the II state. This allows computation of the correct ΔG_p contribution for multivalent iron when the Fe_2O_3 molar concentration is used for durability prediction. However, in the current implementation of the control strategy for the DWPF ϕ_{Fe} is assumed to be 0.

8.0 PCCS Sample Calculation

In this section, a sample calculation of the SME Acceptability Determination is provided. Table 8-1 provides the starting place for these calculations – a set of chemical composition measurements generated from a collection of n=4 SME samples. The last column of the table provides the average of the 4 samples and it is this composition that is to be assessed in the illustrative calculation.

† The ratio of reduced to total copper is assumed to be known and thus has no variance contribution.

Table 8-1 Average Chemical Composition Used in Sample Calculations

Element/ Anion	Unit of Measure	Sample Data 1	2	3	4		Average
SME Solids	wt%	48	49	50	49		49
Calcined Solids	wt%	44	46	46	44		45
Spec Gravity	g/mL	1.453	1.427	1.431	1.389		1.4250
Al	wt%	3.175	3.306	3.241	3.372		3.2734
B	wt%	1.821	1.896	1.858	1.933		1.8768
Ba	wt%	0.133	0.139	0.136	0.142		0.1374
Ca	wt%	0.677	0.705	0.691	0.719		0.6977
Ce	wt%	0.113	0.118	0.115	0.120		0.1164
Cr	wt%	0.105	0.110	0.108	0.112		0.1087
Cs	wt%	0.450	0.468	0.459	0.478		0.4637
Cu	wt%	0.079	0.083	0.081	0.084		0.0817
Fe	wt%	5.421	5.644	5.533	5.756		5.5886
K	wt%	0.110	0.114	0.112	0.117		0.1132
La	wt%	0.085	0.088	0.086	0.090		0.0872
Li	wt%	1.471	1.532	1.501	1.562		1.5165
Mg	wt%	0.418	0.435	0.427	0.444		0.4311
Mn	wt%	1.478	1.539	1.509	1.570		1.5241
Mo	wt%	0	0	0	0		0.0000
Na	wt%	9.513	9.905	9.709	10.101		9.8072
Nd	wt%	0	0	0	0		0.0000
Ni	wt%	0.661	0.688	0.674	0.702		0.6812
Pb	wt%	0.123	0.128	0.125	0.130		0.1266
Si	wt%	23.408	24.373	23.890	24.856		24.1316
Th	wt%	0.475	0.494	0.485	0.504		0.4895
Ti	wt%	1.025	1.067	1.046	1.088		1.0562
U	wt%	2.426	2.526	2.476	2.576		2.5012
Y	wt%	0	0	0	0		0.0000
Zn	wt%	0.080	0.083	0.081	0.085		0.0822
Zr	wt%	0.098	0.102	0.100	0.104		0.1010
Cl	ppm[♣]	0	0	0	0		0.0000
F	ppm	0	0	0	0		0.0000
HCOO	ppm	0	0	0	0		0.0000
NO_2	ppm	100	100	100	100		100.0000
NO_3	ppm	100	100	100	100		100.0000
PO_4	ppm	100	100	100	100		100.0000
SO_4	ppm	595.2	619.8	607.5	632.1		613.6516
TOC	ppm	0	0	0	0		0.0000

[♣] ppm = parts per million

Using the information of Table 8-1 and the gravimetric factors and molecular weights as directed in Table A2 of Appendix A, the corresponding molar oxide concentrations can be calculated. This is accomplished for each element whose concentration is reported in wt% by multiplying the wt% value by the appropriate gravimetric factor and dividing by the molecular weight of the corresponding oxide. For each anion of Table 8-1 (reported in parts per million, ppm), the determination of the corresponding molar concentration is conducted using the calcined wt% solids (the average measurement from Table 8-1) as discussed in Appendix A. That is, the ppm value of the anion is divided by 100 times the calcined wt% solids value; then, the result is multiplied by the appropriate gravimetric factor for the anion or anion group and divided by the molecular weight of the corresponding anion or anion group to compute the desired molar concentration. As a final comment on the determination of the molar concentrations for the SME batch, note that the components HCOO, NO_2, and NO_3 are not used by the control system (i.e., these constituents are not used in the PCCS calculations). More specifically, these constituents are not involved in any way in any of the constraints (process, product, or solubility) associated with PCCS.

Table 8-2 Molar Oxide/Anion Group Concentration for Sample Calculation

Oxide	Molar Concentration	Oxide	Molar Concentration
Al_2O_3	0.06066	MoO_3	0.00000
B_2O_3	0.08681	NO_2	0.70016
BaO	0.00100	NO_3	0.00000
HCOO	0.05811	Na_2O	0.21330
CaO	0.01742	Na_2SO_4	0.00142
Ce_2O_3	0.00042	Nd_2O_3	0.00000
NaCl	0.00000	NiO	0.01160
Cr_2O_3	0.00105	P_2O_5	0.00012
Cs_2O	0.00174	PbO	0.00061
CuO	0.00129	SiO_2	0.85920
NaF	0.00000	ThO_2	0.00211
Fe_2O_3	0.05003	TiO_2	0.02206
K_2O	0.00145	U_3O_8	0.00350
La_2O_3	0.00031	Y_2O_3	0.00000
Li_2O	0.10928	ZnO	0.00126
MgO	0.01773	ZrO_2	0.00111
MnO	0.02774		

In the preceding discussions, the vector $\underline{z}$ was used to represent, for a given SME batch, the average molar oxide concentrations, such as those provided in Table 8-2. For each of the constraints except for T_L, the PAR evaluation for the constraint involves a linear combination of the $\underline{z}$ vector and a corresponding offset in the form of an inequality. Equation 2 provides the general form for each of these inequalities, and Table 8-3 provides the $\underline{a}$ vectors and the β's (the offsets) that complete the information necessary to evaluate the PAR limits for these constraints.

Using the approach of Appendix B for each of these constraints (i.e., all of the constraints except T_L), the MAR limit is defined as:

Equation 104

$$\underline{z}\underline{a}^T - \beta - t_\alpha(m-1)\sqrt{\frac{\underline{a}\mathbf{S}\underline{a}^T}{n}} \geq 0$$

where $t_\alpha(m\text{-}1)$ represents the upper 100 α% tail of the Student's t distribution with m-1 degrees of freedom and

Equation 105

$$\frac{\underline{a}\mathbf{S}\underline{a}^T}{n} \equiv \text{maximum}\left[\begin{array}{l}\dfrac{(\underline{a})\mathbf{S}_m(\underline{a})^T}{n} = \dfrac{1}{n}\displaystyle\sum_{j=0}^{q-1}\sum_{k=0}^{q-1}(\underline{a})_j(\underline{a})_k(\mathbf{S}_m)_{j,k} \\ \dfrac{(\underline{a})\mathbf{S}_n(\underline{a})^T}{n} = \dfrac{1}{n}\displaystyle\sum_{j=0}^{q-1}\sum_{k=0}^{q-1}(\underline{a})_j(\underline{a})_k(\mathbf{S}_n)_{j,k}\end{array}\right]$$

with S_m and S_n representing the covariance matrices (an absolute error structure based upon historical data versus a relative error structure based upon the current $\underline{z}$ vector, respectively) as described in Appendix B.

To illustrate the calculations, the MAR limits are computed both for the absolute-error model using the "historical" data of Table B2 in Appendix B as

Equation 106

$$MAR_{Historical} = \beta + t_\alpha(m-1)\sqrt{\frac{\underline{a}\mathbf{S}_m\underline{a}^T}{n}} \geq 0$$

and for the relative-error model using the "current" (i.e., $\underline{z}$) data of Table 8-2 as

Equation 107

$$MAR_{Current} = \beta + t_\alpha(m-1)\sqrt{\frac{\underline{a}\mathbf{S}_n\underline{a}^T}{n}} \geq 0$$

The larger of these two values for each constraint is selected as the MAR limit, and the derived value, $\underline{z}\underline{a}^T$, for each constraint is compared to its MAR limit:

$$\text{if } \underline{z}\underline{a}^T - \text{MAR} = \text{MAR difference} > 0,$$

then the composition satisfies the MAR limit for the given constraint.

Table 8-4 provides the result of these calculations for all of the constraints except for T_L.

Table 8-3 Vector Columns and PAR Limits (Offsets, β's, in the last row) for All Constraints Except for T_L

	B	Li	Na	High	Low		Low	High										
Oxide	Leaching	Leaching	Leaching	Viscosity	Viscosity	Al_2O_3	Conserv	Conserv	Al_2O_3	TiO_2	TiO_2	NaCl	NaF	Cr_2O_3	Na_2SO_4	Cu	R_2O	Neph
Al_2O_3	37.680	37.680	37.680	-2	2	101.961	101.9621	-101.9612	101.961	0	0	0	0	0	0	0	0	-63.2159
B_2O_3	-10.430	-10.430	-10.430	1	-1	0	69.6202	-69.6202	0	0	0	0	0	0	0	0	0	0
BaO	-23.180	-23.180	-23.180	0	0	0	153.3394	-153.3394	0	0	0	0	0	0	0	0	0	0
HCOO	0.000	0.000	0.000	0	0	0	0.0000	0.0000	0	0	0	0	0	0	0	0	0	0
CaO	-13.790	-13.790	-13.790	0	0	0	56.0794	-56.0794	0	0	0	0	0	0	0	0	0	0
Ce_2O_3	-44.990	-44.990	-44.990	0	0	0	328.2382	-328.2382	0	0	0	0	0	0	0	0	0	0
NaCl	0.000	0.000	0.000	0	0	0	0.0000	0.0000	0	0	0	-58.4428	0	0	0	0	0	0
Cr_2O_3	11.950	11.950	11.950	0	0	0	151.9902	-151.9902	0	0	0	0	0	-151.9902	0	0	0	0
Cs_2O	-80.380	-80.380	-80.380	2	-2	0	281.8094	-281.8094	0	0	0	0	0	0	0	0	-281.8094	0
CuO	-4.955	-4.955	-4.955	0	0	0	75.5439	-75.5439	0	0	0	0	0	0	0	-63.5383	0	0
NaF	0.000	0.000	0.0000	0	0	0	0.0000	0.0000	0	0	0	0	-41.9882	0	0	0	0	0
Fe_2O_3	14.560	14.560	14.560	2	-2	0	159.6922	-159.6922	0	0	0	0	0	0	0	0	0	0
K_2O	-76.410	-76.410	-76.410	2	-2	0	94.2034	-94.2034	0	0	0	0	0	0	0	0	-94.2034	0
La_2O_3	-48.590	-48.590	-48.590	0	0	0	325.8182	-325.8182	0	0	0	0	0	0	0	0	0	0
Li_2O	-24.040	-24.040	-24.040	2	-2	0	29.8774	-29.8774	0	0	0	0	0	0	0	0	-29.8774	0
MgO	-6.570	-6.570	-6.570	0	0	0	40.3114	-40.3114	0	0	0	0	0	0	0	0	0	0
MnO	-24.440	-24.440	-24.440	0	0	0	70.9374	-70.9374	0	0	0	0	0	0	0	0	0	0
MoO_3	16.460	16.460	16.460	0	0	0	143.9382	-143.9382	0	0	0	0	0	0	0	0	0	0
NO_2	0.000	0.000	0.000	0	0	0	0.0000	0.0000	0	0	0	0	0	0	0	0	0	0
NO_3	0.000	0.000	0.000	0	0	0	0.0000	0.0000	0	0	0	0	0	0	0	0	0	0
Na_2O	-53.090	-53.090	-53.090	2	-2	0	61.9790	-61.9790	0	0	0	0	0	0	0	0	-61.9790	-38.4270
Na_2SO_4	0.000	0.000	0.000	0	0	0	0.0000	0.0000	0	0	0	0	0	0	-142.0412	0	0	0
Nd_2O_3	-37.790	-37.790	-37.790	0	0	0	336.4782	-336.4782	0	0	0	0	0	0	0	0	0	0
NiO	0.370	0.370	0.370	0	0	0	74.7094	-74.7094	0	0	0	0	0	0	0	0	0	0
P_2O_5	-26.550	-26.550	-26.550	0	0	0	141.9446	-141.9446	0	0	0	0	0	0	0	0	0	0
PbO	21.050	21.050	21.050	0	0	0	223.1894	-223.1894	0	0	0	0	0	0	0	0	0	0
SiO_2	4.050	4.050	4.050	-0.79548	1.200566	0	60.0848	-60.0848	0	0	0	0	0	0	0	0	0	22.8322
ThO_2	19.230	19.230	19.230	0	0	0	264.0368	-264.0368	0	0	0	0	0	0	0	0	0	0
TiO_2	16.270	16.270	16.270	1	-1	0	79.8988	-79.8988	0	-79.8988	-79.8988	0	0	0	0	0	0	0
U_3O_8	-23.770	-23.770	-23.770	0	0	0	842.0852	-842.0852	0	0	0	0	0	0	0	0	0	0
Y_2O_3	-12.910	-12.910	-12.910	0	0	0	225.8082	-225.8082	0	0	0	0	0	0	0	0	0	0
ZnO	0.920	0.920	0.920	0	0	0	81.3694	-81.3694	0	0	0	0	0	0	0	0	0	0
ZrO_2	17.490	17.490	17.490	0	0	0	123.2188	-123.2188	0	0	0	0	0	0	0	0	0	0
PAR(β)	-14.395	-14.248	-14.476	0	0	3.0	95	-105	4.0	-2.0	-6.0	-1.0	-1.0	-0.30	-0.59	-0.50	-19.3	0

Table 8-4 Results of Sample Calculations for All Constraints Except T_L

	PCCS Constraint	Historical Error Model MAR Limit	Current Error Model MAR Limit	MAR Limit	Derived Value for Constraint	MAR Diff	Constraint Status	Process/ Property Value	Property Unit of Measure
	B Leaching	-14.009	-14.098	-14.0092	-9.3480	4.6610	Met	0.607	g/L
	Li Leaching	-13.862	-13.951	-13.862	-9.3480	4.5141	Met	0.655	g/L
	Na Leaching	-14.090	-14.179	-14.090	-9.3480	4.7421	Met	0.617	g/L
High	Viscosity	0.012	0.014	0.0139	0.0557	0.0417	Met	81.294	poise
Low	Viscosity	0.026	0.029	0.0294	0.2924	0.2630	Met	81.294	poise
	$Al_2O_3 \geq 3$	3.184	3.271	3.271	6.185	2.914	Met	6.185	wt% oxide
Low	Conservation	95	95	95	99.7899	4.7899	Met	99.7899	wt% oxide
High	Conservation	-105	-105	-105	-99.7899	5.2101	Met	99.7899	wt% oxide
	$Al_2O_3 \geq 4$	4.184	4.271	4.271	6.185	1.914	Not Required	6.185	wt% oxide
ROC Constraint	$TiO_2 \leq 2$	-1.983	-1.932	-1.932	-1.7622	0.1695	Met	1.7622	wt% oxide
Model Limit Constraint	$TiO_2 \leq 6.0$	-5.983	-5.932	-5.9318	-1.7622	4.1695	Met	1.7622	wt% oxide
	NaCl solubility	-1.000	-1.000	-1.000	0.000	1.000	Met	0.000	wt% oxide
	NaF solubility	-1.000	-1.000	-1.000	0.000	1.000	Met	0.000	wt% oxide
	Cr_2O_3 solubility	-0.273	-0.254	-0.254	-0.159	0.095	Met	0.159	wt% oxide
	Na_2SO_4 solubility	-0.590	-0.590	-0.590	-0.202	0.388	Met	0.202	wt% oxide
	Cu solubility	-0.488	-0.496	-0.487	-0.082	0.406	Met	0.082	wt% oxide
	R_2O	-18.641	-18.683	-18.641	-17.113	1.528	Not Required	17.113	wt% oxide
	Nepheline	0.678	0.642	0.678	7.586	6.908	Met	0.727	ratio

Recall from Section 6.3.1 that there are options for satisfying the homogeneity constraint, and these depend on the average measured concentration of TiO_2 from the SME samples:

If $TiO_2 \leq 2$ wt% (with MU applied),

then

Equation 108
$$\underline{z}\,\underline{a}^{T}_{Al_2O_3-1} - 3.0 - t_{\alpha}(m-1)\sqrt{\frac{\underline{a}_{Al_2O_3-1}\mathbf{S}\,\underline{a}^{T}_{Al_2O_3-1}}{n}} \geq 0$$

and

Equation 109
$$\underline{z}\,\underline{a}^{T}_{alkali} - (-19.3) - t_{\alpha}(m-1)\sqrt{\frac{\underline{a}_{alkali}\mathbf{S}\,\underline{a}^{T}_{alkali}}{n}} \geq 0$$

where the vector and offset associated with the alkali content of the composition are provided in Table 6-3.

or

Equation 110
$$\underline{z}\,\underline{a}^{T}_{Al_2O_3-2} - 4.0 - t_{\alpha}(m-1)\sqrt{\frac{\underline{a}_{Al_2O_3-2}\mathbf{S}\,\underline{a}^{T}_{Al_2O_3-2}}{n}} \geq 0$$

Else

Equation 111
$$\underline{z}\,\underline{a}^{T}_{Al_2O_3-2} - 4.0 - t_{\alpha}(m-1)\sqrt{\frac{\underline{a}_{Al_2O_3-2}\mathbf{S}\,\underline{a}^{T}_{Al_2O_3-2}}{n}} \geq 0$$

Note that the derived value for TiO_2 is 1.762, and thus the constraint $TiO_2 \leq 2$ wt% is met even after MU is applied. The derived value for the alumina constraint is 6.185, and this value is greater than 3.0 plus MU (i.e., the MAR limit for the alumina constraint) which equals 3.271 (i.e., the MU is 0.271). Also, note that this implies that 4.0 plus the MU would be 4.0 + 0.271 = 4.271. Since the derived value (6.185) is greater than 4.271 the second option is satisfied, but since TiO_2 is less than 2 wt% and R_2O is less than 19.3 wt%, this second constraint on the Al_2O_3 concentration is not required. As was just noted, the derived value -17.113 for the R_2O (sum of alkali) constraint is greater than its MAR limit of –18.641 (i.e., the alkali MAR is satisfied). Thus, homogeneity for this composition is satisfied, leaving only the T_L constraint.

The nonlinearity of the T_L model (and corresponding constraint) forces it to be handled in a manner that differs from the way that was just used for the other constraints. First of all, using the molar oxide concentrations (z**.**) from Table 8-1 and the ϕ's (speciation values) from Table 6-10, compute the estimated T_L in ºC for the SME batch using:

Equation 112
$$\frac{1}{T_L(K)} = \ln\left\{(M_2)^a (M_1)^b (M_T)^c\right\} + d = a\ln(M_2) + b\ln(M_1) + c\ln(M_T) + d$$

or

Equation 113 $$T_L(^\circ C) = \{a\ln(M_2) + b\ln(M_1) + c\ln(M_T) + d\}^{-1} - 273$$

where

$$\Sigma_{MT} \equiv \phi_{MT,SiO_2} z_{SiO_2} + \phi_{MT,Al_2O_3} z_{Al_2O_3} + \phi_{MT,Fe_2O_3} z_{Fe_2O_3}$$

$$\Sigma_{M1} \equiv \phi_{M1,Al_2O_3} z_{Al_2O_3} + \phi_{M1,Fe_2O_3} z_{Fe_2O_3} + \phi_{M1,TiO_2} z_{TiO_2} + \phi_{M1,Cr_2O_3} z_{Cr_2O_3} + \phi_{M1,ZrO_2} z_{ZrO_2} + \phi_{M1,NiO} z_{NiO} + \phi_{M1,MgO} z_{MgO} + \phi_{M1,MnO} z_{MnO}$$

$$\Sigma_{M2} \equiv \phi_{M2,NiO} z_{NiO} + \phi_{M2,MgO} z_{MgO} + \phi_{M2,MnO} z_{MnO} + \phi_{M2,CaO} z_{CaO} + \phi_{M2,K_2O} z_{K_2O} + \phi_{M2,Li_2O} z_{Li_2O} + \phi_{M2,Na_2O} z_{Na_2O}$$

$$\Sigma_{T1} \equiv \phi_{T1,SiO_2} z_{SiO_2} + \phi_{T1,Al_2O_3} z_{Al_2O_3} + \phi_{T1,Fe_2O_3} z_{Fe_2O_3} + \phi_{T1,TiO_2} z_{TiO_2}$$

$$\Sigma_{N1} \equiv \phi_{N1,K_2O} z_{K_2O} + \phi_{N1,Li_2O} z_{Li_2O} + \phi_{N1,Na_2O} z_{Na_2O}$$

and

$$M_2 \equiv \frac{\Sigma_{M2}}{\Sigma}, M_1 \equiv \frac{\Sigma_{M1}}{\Sigma}, M_T \equiv \frac{\Sigma_{MT}}{\Sigma}, \text{and } \Sigma \equiv \Sigma_{M2} + \Sigma_{M1} + \Sigma_{MT} + \Sigma_{T1} + \Sigma_{N1}$$

The predicted T_L is 963.1ºC.

The assessment of the SME composition against the T_L PAR limit (in $1/T_L(K)$) can be conducted (as discussed in Section 6.5.1) using

Equation 114

$$\ln\left\{(M_2)^{-0.000353617}(M_1)^{-0.000691213}(M_T)^{-0.000389016}\right\} - 0.002023544$$

$$-\left(2.41717x10^{-5}\right)\sqrt{pF_{2\alpha}(p,N-p)}\sqrt{\xi\begin{bmatrix} 142 & -188.873614 & -388.925653 & -157.601204 \\ -188.873614 & 254.982966 & 515.389786 & 208.284252 \\ -388.925653 & 515.389786 & 1069.743318 & 428.191038 \\ -157.601204 & 208.284252 & 428.191038 & 181.683573 \end{bmatrix}^{-1}\xi^T}$$

$$\geq 7.56x10^{-4}K^{-1}$$

where ξ is defined to be the vector (i.e., [1 $\ln(M_2)$ $\ln(M_1)$ $\ln(M_T)$]) of values at which to predict $(1/T_L)$, p=4, and n=142, α=0.05 (or 5%), and $F_{0.10}(4,138)$=1.986045. Thus, for the given SME composition, compute the values of $\ln(M_2)$, $\ln(M_1)$, and $\ln(M_T)$ and see whether this inequality is satisfied. If so, the composition is in the T_L PAR.

For the composition of Table 8-2, the PAR limit is 1038.70ºC. Note that the predicted T_L of 963.1ºC is less than (and thus, satisfies) this PAR limit.

Next, the T_L MAR limits for the historical (absolute error model) and the current (relative-error model) compositions are computed as directed in Section 6.5.2 yielding:

$MAR_{historical}$ = 1012.93ºC and $MAR_{current}$ = 1004.71ºC

Thus, the MAR limit is the smaller of the two or 1004.71ºC, and since the predicted T_L of 963.1ºC is less than this value, the composition satisfies the T_L MAR.

Thus, the SME composition of Table 8-1 satisfies all of the appropriate MAR limits at the appropriate confidence levels and thus, would be considered acceptable.

9.0 Path Forward and Recommendations

The path forward to support the implementation of these changes for use during DWPF operations includes:

- Develop, with input from DWPF & Saltstone Facility Engineering (D&S-FE), test cases for the revision to support the necessary modifications to the web-based PCCS,
- Work with the D&S-FE and Information Technology organization to support the modification of the web-based implementation of PCCS, and
- Incorporate the changes detailed in this report into future frit development efforts for DWPF processing with SWPF operational.

10.0 Conclusions

This document establishes the technical basis for the DWPF PCCS, a statistical process control system for monitoring SME batches and for supporting acceptability decisions at this production hold-point for the facility. Using chemical composition measurements derived from SME samples as input, the system assesses the acceptability of the SME batch against appropriate process, product quality, and solubility constraints after accounting for applicable uncertainties (those due to property models, when such models are used, and those due to sample measurements themselves).

This report meticulously details the measurement inputs, the property models, and the statistical methods for dealing with their uncertainties in meeting the constraints imposed on DWPF operations. The system implements each of the constraints associated with product quality (i.e., the durability of the waste form produced by the DWPF) at the required 95% confidence level. The confidence levels for meeting the other constraints (i.e., those associated with process-ability and solubility), while not mandated to be at 95%, were developed to this confidence level in this paper. However, the system does allow flexibility, at management's discretion, in the confidence levels associated with these non-waste-form-affecting constraints.

This is the sixth revision of the SME Acceptability Determination report, and it establishes the technical basis necessary for the modification of PCCS that is planned to occur prior to the integration of the SWPF into the DWPF flowsheet. It should also be noted that this revision is also a technical basis for PCCS for sludge-only processing at the DWPF; should that mode of processing become necessary after SWPF becomes operational.

11.0 References

[1] Fox, K.M., T.B. Edwards, and C.M. Jantzen, "Task Technical and Quality Assurance Plan for SWPF Integration into the DWPF – Glass Property/Model Impacts," SRNL-RP-2014-00348, Revision 1, 2017.

[2] Windham J.P. "Slurry Mix Evaporator (SME) Tank Acceptability Report," X-TTR-S-00053, Revision 1, 2017.

[3] Jantzen, C.M, J.B. Pickett, K.G. Brown, T.B. Edwards, and D.C. Beam, "Process/Product Models for the Defense Waste Processing Facility (DWPF): Part I. Predicting Glass Durability from Composition Using a Thermodynamic Hydration Energy Reaction Model (THERMO) (U)," WSRC-TR-93-672, Revision 1, 1995.

[4] Office of Environmental Management, "Waste Acceptance Product Specifications for Vitrified High-Level Waste Forms WAPS," USDOE Document DOE/EM-0093, Revision 2, U.S. Department of Energy, Germantown, MD, 1996.

[5] ASTM C1285-14, "Standard Test Methods for Determining Chemical Durability of Nuclear, Hazardous, and Mixed Waste Glasses and Multiphase Glass Ceramics: The Product Consistency Test (PCT)," Annual Book of ASTM Standards, Volume 12.01, 2014.

[6] Brown, K.G. and T.B. Edwards, "Definition of the DWPF Predictability Constraint (U)," WSRC-TR-95-0060, Revision 0, 1995.

[7] Edwards, T.B. and K.G. Brown, "Evaluating the Glasses Batched for the Tank 42 Variability Study (U)," SRT-SCS-98-017, Revision 0, 1998.

[8] Brown, K.G. "Relaxation of the Lower Frit Loading Constraint for DWPF Process Control (U)," WSRC-RP-99-00355, Revision 0, 1999.

[9] Smith, M.E. "Reevaluation of DWPF High Viscosity Constraint: SRTC ITS Position," SRT-GFM-99-0011, 1999.

[10] Brown, K.G. "Changes Made to the DWPF PCCS Spreadsheet (U)," SRTC-GPD-2002-00059, 2002.

[11] Peeler, D.K., C.C. Herman, M.E. Smith, T.H. Lorier, D.R. Best, T.B. Edwards, and M.A. Baich, "An Assessment of the Sulfate Solubility Limit for the Frit 418 – Sludge Batch 2/3 System," WSRC-TR-2004-00081, Revision 0, 2004.

[12] Herman, C.C., T.B. Edwards, D.R. Best, D.M. Marsh, and R.J. Workman, "Reduction of Constraints: Phase 2 Experimental Assessment for Sludge-Only Processing," WSRC-TR-2002-00482, Revision 0, 2002.

[13] Raszewski, F.C. and T.B. Edwards, "Reduction of Constraints for Coupled Operations," SRNL-STI-2009-00465, Revision 0, 2009.

[14] Jantzen, C.M., T.B. Edwards, and C.L. Trivelpiece, “Defense Waste Processing Facility (DWPF) Durability-Composition Models and the Applicability of the Associated Reduction of Constraints (ROC) Criteria for High TiO_2 Containing Glasses,” SRNL-STI-2016-00372, Revision 0, 2016.

[15] Plodinec, M.J. and G.W. Wilds, "Long-Term Waste Management Progress Report Role of TiO_2 in SRP Waste Glasses," DPST-78-358, 1978.

[16] Lorier, T.H. and C.M. Jantzen, “Evaluation of the TiO_2 Limit for DWPF Glass,” WSRC-TR-2003-00396, Revision 0, 2003.

[17] Peeler, D.K. and T.B. Edwards, “SWPF Integration into the DWPF Flowsheet: Development of a Glass Test Matrix to Fill Compositional Gaps,” SRNL-L3100-2014-00200, 2014.

[18] Jantzen, C.M. and T.B. Edwards, “Defense Waste Processing Facility (DWPF) Viscosity Model: Revisions for Processing High TiO_2 Containing Glasses,” SRNL-STI-2016-00115, Revision 0, 2016.

[19] Jantzen, C.M., T.B. Edwards, and C.L. Trivelpiece, “Defense Waste Processing Facility (DWPF) Liquidus Model: Revisions for Processing Higher TiO_2 Containing Glasses,” SRNL-STI-2017-00016, Revision 0, 2017.

[20] Jantzen, C.M. “Sulfate and Halide Salt Solubility and DWPF Processing,” SRNL-STI-2013-00690, 2013.

[21] Bickford, D.F., P. Hrma, B.W. Bowen, and P.K. Smith, "Control of Radioactive Waste-Glass Melters: Parts 1 and 2," DP-MS-86-217-AI & II, 1987.

[22] Bickford, D.F. and C.M. Jantzen, "Inhibitor Limits for Washed Precipitate Based on Glass Quality and Solubility Limits," DPST-86-546, 1986.

[23] Ramsey, W.G. and R.F. Schumacher, "Effects of Formate and Nitrate Concentration on Waste Glass Redox at High Copper Concentration (U)," WSRC-TR-92-484, Revision 0, 1992.

[24] Edwards, T.B., D.K. Peeler, and S.L. Marra, “Revisiting the Prediction Limits for Acceptable Durability (U),” WSRC-TR-2003-00510, Revision 0, 2003.

[25] Jantzen, C.M., N.E. Bibler, D.C. Beam, C.L. Crawford, and M.A. Pickett, “Characterization of the Defense Waste Processing Facility (DWPF) Environmental Assessment (EA) Glass Standard Reference Material (U),” WSRC-TR-92-346, Revision 1, 1993.

[26] Miller, Jr., R.G. **Simultaneous Statistical Inference**, Second Edition, Springer-Verlag, New York, 1981.

[27] Edwards, T.B., D.K. Peeler, and K.M. Fox, “The Nepheline Discriminator: Justification and DWPF PCCS Implementation Details,” WSRC-STI-2006-00014, Revision 0, 2006.

[28] Li, H., P. Hrma, J.D. Vienna, M. Qian, Y. Su, and D.E. Smith, “Effects of Al_2O_3, B_2O_3, Na_2O, and SiO_2 on Nepheline Formation in Borosilicate Glasses: Chemical and Physical Correlations,” **Journal of Non-Crystalline Solids**, 331 [1-3], pgs. 202 – 216, 2003.

[29] Peeler, D.K., T.B. Edwards, I.A. Reamer, and R.J. Workman, "Nepheline Formation Study for Sludge Batch 4 (SB4): Phase 1 Experimental Results," WSRC-TR-2005-00371, Revision 0, 2005.

[30] Peeler, D.K., T.B. Edwards, D.R. Best, I.A. Reamer, and R.J. Workman, "Nepheline Formation Study for Sludge Batch 4 (SB4): Phase 2 Experimental Results," WSRC-TR-2006-00006, Revision 0, 2006.

[31] Fox, K.M., T.B. Edwards, D.K. Peeler, D.R. Best, I.A. Reamer, and R.J. Workman, "Nepheline Formation Study for Sludge Batch 4 (SB4): Phase 3 Experimental Results," WSRC-TR-2006-00093, Revision 0, 2006.

[32] Fox, K.M., T.B. Edwards, D.K. Peeler, D.R. Best, I.A. Reamer, and R.J. Workman, "Durability and Nepheline Crystallization Study for High Level Waste (HLW) Sludge Batch 4 (SB4) Glasses Formulated with Frit 503," WSRC-STI-2006-00009, Revision 0, 2006.

[33] Marra, S.L. and C.M. Jantzen, "Characterization of Projected DWPF Glass Heat Treated to Simulate Canister Centerline Cooling (U)," WSRC-TR-92-142, Revision 1, 1993.

[34] Jantzen, C.M. "The Impacts of Uranium and Thorium on the Defense Waste Processing Facility (DWPF) Viscosity Model (U)," WSRC-TR-2004-00311, Revision 0, 2005.

[35] Edwards, T.B. and D.K. Peeler, "The Information Needed to Change PCCS to Support the Implementation of the New Viscosity Model and the Impact of the New Model on DWPF's Operating Windows," SRNL-SCS-2005-00054, 2005.

[36] Scheffé, H. **The Analysis of Variance**, John Wiley & Sons, New York, 1959.

[37] Draper, N.R. and H. Smith, **Applied Regression Analysis**, Second Edition, John Wiley & Sons, New York, 1981.

[38] Brown, K.G., C.M. Jantzen, and G. Ritzhaupt, "Relating Liquidus Temperature to Composition for Defense Waste Processing Facility (DWPF) Process Control (U)," WSRC-TR-2001-00520, Revision 0, 2001.

[39] Schrieber, H.D. and A.L. Hockman, "Redox Chemistry in Candidate Glasses for Nuclear Waste Immobilization," **Journal of the American Ceramic Society,** 70 [8], pgs. 591-594, 1987.

[40] Schreiber, H.D., P.G. Leonhard, R.G. Nofsinger, M.W. Henning, C.W. Schreiber, and S.J. Kozak, "Oxidation-Reduction Chemistry of NonMetals in a Reference Borosilicate Melt," **Advances in the Fusion of Glass**, D.F. Bickford, F.E. Woolley, W.E. Horsfall, E.N. Boulos, J.N. Lingscheit, F. Harding, F. Olix, W.C. LaCourse, and L.D. Pye (Eds.), The American Ceramic Society, Inc., Westerville, OH, pgs. 29.1-29.14, 1988.

[41] Jantzen, C.M., J.R. Zamecnik, D.C. Koopman, C.C. Herman, and J.B. Pickett, "Electron Equivalents Model for Controlling REDuction-Oxidation (REDOX) Equilibrium During High Level Waste (HLW) Vitrification," WSRC-TR-2003-00126, Revision 0, 2003.

[42] Cozzi, A.D., T.B. Edwards, D.K. Peeler, and D.R. Best, "Impact of REDOX on Durability for Sludge Batch 2 Part II: Experimental Results and Recommendations," WSRC-TR-2003-00246, Revision 0, 2003.

[43] Graybill, F.A. **An Introduction to Linear Statistical Models**, Vol I, McGraw-Hill, New York, Theorem 3.6, pg. 56, 1961.

[44] Morrison, D.F. **Multivariate Statistical Methods**, Second Edition, McGraw-Hill, New York, pg. 130, 1976.

[45] Reeve, C.P. "Statistical Analysis of DWPF Prototypic Tests: SME Feed (U)," SCS-ASG-93-0050, 1993.

[46] Reeve, C.P. "PCCS Covariance Matrices Based on Prototypic Tests (U)," SCS-ASG-93-0048, 1993.

Appendix A. Chemical Composition Measurements of Slurry Mix Evaporator (SME) Samples

This appendix identifies the measurements derived from the SME samples and establishes a unit of measurement for component concentrations that is to be used in PCCS calculations.

SME Sample Measurements

The acceptability determination for a SME batch by PCCS is initiated by the entry of measurements from n (where $n \geq 4$) samples taken from the contents of the SME. The measurements generated from each of the SME samples are outlined in Table A1. As noted in this table, measurements are provided for the physical properties of total wt% solids, the calcined wt% solids, and specific gravity (in g/mL). The remaining rows of Table A1 indicate the components that are used to represent the chemical composition of the sample. This is the largest set of components deemed necessary to capture the information needed for waste solubility constraints as well as that needed to cover components whose concentrations in the DWPF glass product would be expected to exceed 0.5% by weight [4]. The concentration measurement for each cation reported in Table A1 is given in mass weight percent (wt%).

Table A1. Measurements from Each SME Sample

	Unit of Measure		Unit of Measure		Unit of Measure
Total Solids	wt%	Calcined Solids	wt%	Specific Gravity	g/mL
Element/anion		Element/anion		Element/anion	
Al	wt%	Mg	wt%	Y	wt%
B	wt%	Mn	wt%	Zn	wt%
Ba	wt%	Mo	wt%	Zr	wt%
Ca	wt%	Na	wt%	Cl	ppm
Ce	wt%	Nd	wt%	F	ppm
Cr	wt%	Ni	wt%	HCOO	ppm
Cs	wt%	Pb	wt%	NO_2	ppm
Cu	wt%	Si	wt%	NO_3	ppm
Fe	wt%	Th	wt%	PO_4	ppm
K	wt%	Ti	wt%	SO_4	ppm
La	wt%	U	wt%	TOC	ppm
Li	wt%				

The concentration of each anion, i, necessary for DWPF process control (i.e., $Cl^- \rightarrow NaCl$, $F^- \rightarrow NaF$, $SO_4^- \rightarrow Na_2SO_4$, and $PO_4^{-3} \rightarrow P_2O_5$) is reported in terms of parts per million (ppm), i.e., g i/10^6g sample or p_i. The sample measurement is converted from the sample basis (i.e., ppm or p_i) to the corresponding elemental analysis basis (i.e., g i/100g glass or x_i) using the formula:

Equation 115

$$x_i \equiv \frac{1}{100\omega_c} p_i$$

where ω_c is the measured calcined wt% solids for the sample and x_i for analyte i is in g i/100g glass. This also indicates that the error associated with these converted compositions, the x_i's, has contributions from both p_i and ω_c. This error can be estimated via propagation of error techniques. However, since the contributions of these anions to the non-solubility constraints (e.g., durability, liquidus temperature, etc.) are rather small, only the error in the measured anion concentration is used in PCCS for DWPF process control.

Unit of Measure for Compositions

As the reader progresses through body of this report, it will become apparent, if it is not already, that there is a need to establish a consistent basis (i.e., unit of measurement) for the SME sample results to facilitate their use in PCCS. The unit of measurement selected for this purpose is molar oxide concentrations (i.e., moles oxide/100g glass) using:

Equation 116

$$z_{oxide} \equiv \frac{x_{oxide}}{M_{oxide}}$$

where M_{oxide} is the molecular weight of the oxide and x_{oxide} is the mass weight percent of the oxide. Table A2 provides the associations between the element reported as part of the SME sample results and the corresponding oxide including the gravimetric factor and the molecular weight. Note that several of the entries in Table A2 actually play no role in the SME acceptability decision: HCOO, NO_2, NO_3, and TOC (total organic carbon). That is, these components are not involved in any of the calculations associated with any of the constraints (process, product, or solubility) imposed on the DWPF operation.

Table A2. Elemental Measurements with Corresponding Oxides, Gravimetric Factors, and Molecular Weights

Element/ anion	Measured as	Gravimetric Factor (γ.)	Corresponding Oxide	Molecular Weight (M.)
Al	wt%	1.8895	Al_2O_3	101.9612
B	wt%	3.2199	B_2O_3	69.6202
Ba	wt%	1.1165	BaO	153.3394
Ca	wt%	1.3992	CaO	56.0794
Ce	wt%	1.1713	Ce_2O_3	328.2382
Cr	wt%	1.4616	Cr_2O_3	151.9902
Cs	wt%	1.0602	Cs_2O	281.8094
Cu	wt%	1.2520	CuO♣	79.55
Fe	wt%	1.4297	Fe_2O_3	159.6922
K	wt%	1.2046	K2O	94.2034
La	wt%	1.1728	La_2O_3	325.8182
Li	wt%	2.1529	Li_2O	29.8774
Mg	wt%	1.6581	MgO	40.3114
Mn	wt%	1.2912	MnO	70.9374
Mo	wt%	1.5003	MoO_3	143.9382
Na	wt%	1.3480	Na_2O	61.979
Nd	wt%	1.1664	Nd_2O_3	336.4782
Ni	wt%	1.2725	NiO	74.7094
Pb	wt%	1.0772	PbO	223.1894
Si	wt%	2.1393	SiO_2	60.0848
Th	wt%	1.1379	ThO_2	264.0368
Ti	wt%	1.6680	TiO_2	79.8988
U	wt%	1.1792	U_3O_8	842.0852
Y	wt%	1.2699	Y_2O_3	225.8082
Zn	wt%	1.2448	ZnO	81.3694
Zr	wt%	1.3508	ZrO_2	123.2188
Cl	ppm	1.6485	NaCl	58.4428
F	ppm	2.2101	NaF	41.9882
HCOO	ppm	Not Used	HCOO	Not Used
NO_2	ppm	Not Used	NO_2	Not Used
NO_3	ppm	Not Used	NO_3	Not Used
PO_4	ppm	0.7473	P_2O_5	141.9446
SO_4	ppm	1.4790	Na_2SO_4	142.0412
TOC	ppm	Not Used	TOC is not used in PCCS	

♣ The molecular weight of Cu_2O utilized in Section 7.1 is 143.09.

The components representing the measured sample compositions in the order used in PCCS is provided in Table A3 and this vector is represented by $\underline{z}$ for each sample.

Table A3. Components Representing SME Composition in the Order Used by PCCS

Order	1	2	3	4	5	6	7	8	9	10	11
Oxide	Al_2O_3	B_2O_3	BaO	HCOO	CaO	Ce_2O_3	NaCl	Cr_2O_3	Cs_2O	CuO	NaF
Order	12	13	14	15	16	17	18	19	20	21	22
Oxide	Fe_2O_3	K_2O	La_2O_3	Li2O	MgO	MnO	MoO_3	NO_2	NO_3	Na_2O	Na_2SO_4
Order	23	24	25	26	27	28	29	30	31	32	33
Oxide	Nd_2O_3	NiO	P_2O_5	PbO	SiO_2	ThO_2	TiO_2	U_3O_8	Y_2O_3	ZnO	ZrO_2

Appendix B. Measurement Uncertainty (MU) for Slurry Mix Evaporator (SME) Samples

Appendix B presents the necessary information for handling the measurement (sampling, preparation, and analytical) errors or uncertainties associated with SME sample results.

Historical Information on MU

One type of uncertainty that must be addressed, as part of the SME acceptability decision, is MU associated with the average chemical composition, $\underline{z}$, for each sample. (See Table A3 in Appendix A for a listing of all of the components of $\underline{z}$.) Here measurement includes the processes of sampling and sample preparation as well as actual measurement.

To quantify the MU, the errors in the measurements comprising $\underline{z}$ are presumed to be Gaussian. Given q important elements,[‡‡] the MU is q-variate Gaussian with true mean $\underline{0}$ and covariance matrix Σ. Thus, by not unreasonable presumption, the measurement $\underline{z}$ is also multivariate normal with true mean $\underline{\mu}$ and the same covariance matrix, and thus obeys the probability density:

Equation 117

$$f(\underline{z}) \equiv \left[(2\pi)^q |\Sigma|\right]^{\frac{1}{2}} \exp\left[\left(-\frac{1}{2}\right)(\underline{z}-\underline{\mu})\Sigma^{-1}(\underline{z}-\underline{\mu})^T\right].$$

Presuming the errors in the concentrations of individual constituents to be multivariate Gaussian enables the traditional methods of multivariate normal theory to apply. Let $\underline{z}$ be a current SME batch composition measurement, which estimates its underlying true composition $\underline{\mu}$. If there are q important constituents, $\underline{z}$ is a 1xq array of *measured* molar oxide concentrations (i.e., mole oxide/100g glass) of the constituent oxides:

Equation 118

$$\underline{z} \equiv \left[z_0, z_1, \ldots, z_{q-1}\right]$$

Let $\mathbf{S}_m$ be a covariance matrix estimate from an historic sample of m such measurements.[†] $\mathbf{S}_m$ consists of the variances within and covariances between the q individual oxides:

Equation 119

$$\mathbf{S}_m \equiv \begin{bmatrix} s_{0,0} & s_{0,1} & \cdots & s_{0,q-1} \\ s_{0,1} & s_{1,1} & \cdots & s_{1,q-1} \\ \cdots & \cdots & \cdots & \cdots \\ s_{0,q-1} & s_{1,q-1} & \cdots & s_{q-1,q-1} \end{bmatrix}$$

where the $s_{i,j}$ are the historic sample variances (i=j) and covariances (i≠j). However the available covariance information for the DWPF is based upon elemental information, i.e., $\underline{x}$. This covariance information consists of the variances within and the covariances between the q individual elements and is contained in the matrix $\mathbf{E}_m$:

---

‡‡ That is, of such type and present in such amount as to have non-negligible effect on the properties under consideration.

† Thus $\mathbf{S}_m$ is developed from data excluding the measurements for the current SME batch and possibly other recent ones. The information used to compute $\mathbf{S}_m$ can be updated if necessary.

Equation 120

$$\mathbf{E}_m \equiv \begin{bmatrix} e_{0,0} & e_{0,1} & \cdots & e_{0,q-1} \\ e_{0,1} & e_{1,1} & \cdots & e_{1,q-1} \\ \cdots & \cdots & \cdots & \cdots \\ e_{0,q-1} & e_{1,q-1} & \cdots & e_{q-1,q-1} \end{bmatrix}.$$

In $\mathbf{E}_m$, the $e_{i,j}$ are the historic sample elemental variances and covariances:

Equation 121

$$e_{i,j} = \frac{1}{m-1}\sum_{k=0}^{m-1}\left(x_{i,k} - \bar{x}_i\right)\left(x_{j,k} - \bar{x}_j\right) \quad \text{where} \quad \bar{x}_i = \frac{1}{m}\sum_{k=0}^{m-1} x_{i,k}$$

and $x_{i,k}$ is the elemental mass concentration for the k^{th} element from the i^{th} sample. This covariance matrix may also be defined based upon the correlation matrix, $\mathbf{C}_m$, which consists of the pair-wise correlations between the q individual elements:

Equation 122

$$\mathbf{C}_m \equiv \begin{bmatrix} \rho_{0,0} & \rho_{0,1} & \cdots & \rho_{0,q-1} \\ \rho_{0,1} & \rho_{1,1} & \cdots & \rho_{1,q-1} \\ \cdots & \cdots & \cdots & \cdots \\ \rho_{0,q-1} & \rho_{1,q-1} & \cdots & \rho_{q-1,q-1} \end{bmatrix} \quad \text{where} \quad \rho_{i,j} = \frac{e_{i,j}}{\sqrt{e_{i,i}e_{j,j}}}.$$

Now if $(r_m)_i$ represents the relative standard deviation for the i^{th} element based upon historical information, then:

Equation 123

$$(r_m)_i = \frac{\sqrt{e_{i,i}}}{\bar{x}_i}$$

Therefore, the i,j^{th} member of the historic elemental covariance matrix, $\mathbf{E}_m$, is given by:

Equation 124

$$(\mathbf{E}_m)_{i,j} = e_{i,j} = \left[(r_m)_i \bar{x}_i\right]\left[(r_m)_j \bar{x}_j\right]\rho_{i,j}.$$

Fortunately the elemental covariance matrix, $\mathbf{E}_m$, can be easily transformed to $\mathbf{S}_m$ for SME acceptability determination. The covariance between the i and j^{th} elemental concentrations is defined to be:

Equation 125

$$e_{i,j} \equiv E\left(x_i x_j\right) - E\left(x_i\right)E\left(x_j\right)$$

where E(x) is the expected value or expectation of the parameter x. Similarly, the covariance between the i and j^{th} mass oxide concentrations is:

Equation 126

$$s_{i,j} \equiv E\left(z_i z_j\right) - E\left(z_i\right)E\left(z_j\right).$$

The mass oxide concentration is a simple function of the elemental mass concentration:

Equation 127

$$z_i \equiv \frac{\gamma_i}{M_i} x_i$$

where γ_i is the gravimetric factor converting from mass element to corresponding oxide and M_i is the molecular weight of the corresponding oxide. Thus

Equation 128

$$s_{i,j} \equiv E\left[\left(\frac{\gamma_i}{M_i}x_i\right)\left(\frac{\gamma_j}{M_j}x_j\right)\right] - E\left(\frac{\gamma_i}{M_i}x_i\right)E\left(\frac{\gamma_j}{M_j}x_j\right)$$

or since the expected value of a constant (e.g., γ_i or M_i) is simply the value of the constant:

Equation 129

$$s_{i,j} \equiv \left(\frac{\gamma_i}{M_i}\right)\left(\frac{\gamma_j}{M_j}\right)\left[E(x_i x_j) - E(x_i)E(x_j)\right] = \left(\frac{\gamma_i}{M_i}\right)\left(\frac{\gamma_j}{M_j}\right)e_{i,j}$$

and

Equation 130

$$s_{i,j} = \left[\left(\frac{\gamma_i}{M_i}\right)(r_m)_i \bar{x}_i\right]\left[\left(\frac{\gamma_j}{M_j}\right)(r_m)_j \bar{x}_j\right]\rho_{i,j}.$$

This then provides the information necessary to compute the covariance matrix necessary for SME acceptability determination, $\mathbf{S}_m$, from available historic covariance information. To complete the required information, Tables B1 through B3 are provided. Table B1 provides the elemental correlation matrix derived from historical data. Table B2 provides the average of the historical compositions used to develop this correlation matrix, and Table B3 provides the relative standard deviations of the indicated component for these data.

Note that, for the sake of completeness, there are entries in Tables B1 through B3 for all of the components listed in Table A3. The entries in these tables are zero for the components that are not part of the PCCS calculations and for those components for which no historical data were available.

Table B1. Elemental Correlation Matrix, C_m, for the Corresponding Oxides

	Al_2O_3	B_2O_3	BaO	HCOO	CaO	Ce_2O_3	NaCl	Cr_2O_3	Cs_2O	CuO	NaF	Fe_2O_3	K_2O	La_2O_3	Li_2O	MgO	MnO	MoO_3	NO_2	NO_3	Na_2O	Na_2SO_4	Nd_2O_3	NiO	P_2O_5	PbO	SiO_2	ThO_2	TiO_2	U_3O_8	Y_2O_3	ZnO	ZrO_2
Al_2O_3	1	-0.2133	0	0	0.8997	0	0	-0.1343	0	0.6744	0	0.9335	0.7647	0	0.7009	0.8319	0.9221	0	0	0	0.9128	0	0	0.2892	0	0	0.6898	0	0.8816	0	0	0	0.2669
B_2O_3	-0.2133	1	0	0	-0.1928	0	0	-0.2248	0	-0.148	0	-0.301	0.0697	0	0.1114	-0.0865	-0.268	0	0	0	0.0106	0	0	-0.3906	0	0	0.2229	0	-0.0561	0	0	0	-0.1907
BaO	0	0	0	0	0	0	0	0	0	0	0	0	0	0	0	0	0	0	0	0	0	0	0	0	0	0	0	0	0	0	0	0	0
HCOO	0	0	0	0	0	0	0	0	0	0	0	0	0	0	0	0	0	0	0	0	0	0	0	0	0	0	0	0	0	0	0	0	0
CaO	0.8997	-0.1928	0	0	1	0	0	-0.01	0	0.6031	0	0.7989	0.6906	0	0.6231	0.8488	0.7535	0	0	0	0.7587	0	0	0.3564	0	0	0.6003	0	0.7085	0	0	0	0.3104
Ce_2O_3	0	0	0	0	0	0	0	0	0	0	0	0	0	0	0	0	0	0	0	0	0	0	0	0	0	0	0	0	0	0	0	0	0
NaCl	0	0	0	0	0	0	0	0	0	0	0	0	0	0	0	0	0	0	0	0	0	0	0	0	0	0	0	0	0	0	0	0	0
Cr_2O_3	-0.1343	-0.2248	0	0	-0.01	0	0	1	0	-0.2473	0	-0.0194	-0.2603	0	-0.0721	0.0055	-0.2658	0	0	0	-0.2752	0	0	0.786	0	0	-0.162	0	-0.059	0	0	0	0.536
Cs_2O	0	0	0	0	0	0	0	0	0	0	0	0	0	0	0	0	0	0	0	0	0	0	0	0	0	0	0	0	0	0	0	0	0
CuO	0.6744	-0.148	0	0	0.6031	0	0	-0.2473	0	1	0	0.7322	0.6297	0	0.6401	0.6983	0.7662	0	0	0	0.6998	0	0	0.134	0	0	0.6446	0	0.638	0	0	0	0.1245
NaF	0	0	0	0	0	0	0	0	0	0	0	0	0	0	0	0	0	0	0	0	0	0	0	0	0	0	0	0	0	0	0	0	0
Fe_2O_3	0.9335	-0.301	0	0	0.7989	0	0	-0.0194	0	0.7322	0	1	0.6866	0	0.7226	0.8255	0.9613	0	0	0	0.8852	0	0	0.4147	0	0	0.6753	0	0.9065	0	0	0	0.3327
K_2O	0.7647	0.0697	0	0	0.6906	0	0	-0.2603	0	0.6297	0	0.6866	1	0	0.6065	0.6529	0.7055	0	0	0	0.8244	0	0	0.074	0	0	0.6369	0	0.7135	0	0	0	0.0119
La_2O_3	0	0	0	0	0	0	0	0	0	0	0	0	0	0	0	0	0	0	0	0	0	0	0	0	0	0	0	0	0	0	0	0	0
Li_2O	0.7009	0.114	0	0	0.6231	0	0	-0.0721	0	0.6401	0	0.7226	0.6065	0	1	0.9	0.6678	0	0	0	0.8337	0	0	0.3613	0	0	0.9668	0	0.809	0	0	0	0.3577
MgO	0.8319	-0.0865	0	0	0.8488	0	0	0.0055	0	0.6983	0	0.8255	0.6529	0	0.9	1	0.7514	0	0	0	0.8438	0	0	0.4495	0	0	0.8762	0	0.7873	0	0	0	0.3648
MnO	0.9221	-0.268	0	0	0.7535	0	0	-0.2658	0	0.7662	0	0.9613	0.7055	0	0.6678	0.7514	1	0	0	0	0.8937	0	0	0.1944	0	0	0.6432	0	0.8734	0	0	0	0.1809
MoO_3	0	0	0	0	0	0	0	0	0	0	0	0	0	0	0	0	0	0	0	0	0	0	0	0	0	0	0	0	0	0	0	0	0
NO_2	0	0	0	0	0	0	0	0	0	0	0	0	0	0	0	0	0	0	0	0	0	0	0	0	0	0	0	0	0	0	0	0	0
NO_3	0	0	0	0	0	0	0	0	0	0	0	0	0	0	0	0	0	0	0	0	0	0	0	0	0	0	0	0	0	0	0	0	0
Na_2O	0.9128	0.0106	0	0	0.7587	0	0	-0.2752	0	0.6998	0	0.8852	0.8244	0	0.8337	0.8438	0.8937	0	0	0	1	0	0	0.1507	0	0	0.8456	0	0.8905	0	0	0	0.1403
Na_2SO_4	0	0	0	0	0	0	0	0	0	0	0	0	0	0	0	0	0	0	0	0	0	0	0	0	0	0	0	0	0	0	0	0	0
Nd_2O_3	0	0	0	0	0	0	0	0	0	0	0	0	0	0	0	0	0	0	0	0	0	0	0	0	0	0	0	0	0	0	0	0	0
NiO	0.2892	-0.3906	0	0	0.3564	0	0	0.786	0	0.134	0	0.4147	0.074	0	0.3613	0.4495	0.1944	0	0	0	0.1507	0	0	1	0	0	0.25	0	0.3343	0	0	0	0.713
P_2O_5	0	0	0	0	0	0	0	0	0	0	0	0	0	0	0	0	0	0	0	0	0	0	0	0	0	0	0	0	0	0	0	0	0
PbO	0	0	0	0	0	0	0	0	0	0	0	0	0	0	0	0	0	0	0	0	0	0	0	0	0	0	0	0	0	0	0	0	0
SiO_2	0.6898	0.2229	0	0	0.6003	0	0	-0.162	0	0.6446	0	0.6753	0.6369	0	0.9668	0.8762	0.6432	0	0	0	0.8456	0	0	0.25	0	0	1	0	0.7449	0	0	0	0.2598
ThO_2	0	0	0	0	0	0	0	0	0	0	0	0	0	0	0	0	0	0	0	0	0	0	0	0	0	0	0	0	0	0	0	0	0
TiO_2	0.8816	-0.0561	0	0	0.7085	0	0	-0.059	0	0.638	0	0.9165	0.7135	0	0.809	0.7873	0.8734	0	0	0	0.8905	0	0	0.3343	0	0	0.7449	0	1	0	0	0	0.3595
U_3O_8	0	0	0	0	0	0	0	0	0	0	0	0	0	0	0	0	0	0	0	0	0	0	0	0	0	0	0	0	0	0	0	0	0
Y_2O_3	0	0	0	0	0	0	0	0	0	0	0	0	0	0	0	0	0	0	0	0	0	0	0	0	0	0	0	0	0	0	0	0	0
ZnO	0	0	0	0	0	0	0	0	0	0	0	0	0	0	0	0	0	0	0	0	0	0	0	0	0	0	0	0	0	0	0	0	0
ZrO_2	0.2669	-0.1907	0	0	0.3104	0	0	0.536	0	0.1245	0	0.3327	0.0119	0	0.3577	0.3648	0.1809	0	0	0	0.1403	0	0	0.713	0	0	0.2598	0	0.3595	0	0	0	1

Table B2. Average Historical Elemental Composition (wt%) for the Corresponding Oxides

Al_2O_3	B_2O_3	BaO	HCOO	CaO	Ce_2O_3	NaCl	Cr_2O_3	Cs_2O	CuO	NaF	Fe_2O_3	K_2O	La_2O_3	Li_2O	MgO	MnO	MoO_3	NO_2	NO_3	Na_2O	Na_2SO_4	Nd_2O_3	NiO	P_2O_5	PbO	SiO_2	ThO_2	TiO_2	U_3O_8	Y_2O_3	ZnO	ZrO_2
2.222	2.093	0	0	1.077	0	0	0.064	0	0.25	0	6.235	2.455	0	1.963	0.842	2.111	0	0	0	7.463	0	0	0.643	0	0	23.31	0	0.256	0	0	0	0.029

Table B3. Relative Standard Deviations for Historical Elemental Compositions for the Corresponding Oxides

Al_2O_3	B_2O_3	BaO	HCOO	CaO	Ce_2O_3	NaCl	Cr_2O_3	Cs_2O	CuO	NaF	Fe_2O_3	K_2O	La_2O_3	Li_2O	MgO	MnO	MoO_3	NO_2	NO_3	Na_2O	Na_2SO_4	Nd_2O_3	NiO	P_2O_5	PbO	SiO_2	ThO_2	TiO_2	U_3O_8	Y_2O_3	ZnO	ZrO_2
0.051	0.072	0	0	0.059	0	0	0.335	0	0.058	0	0.048	0.065	0	0.041	0.048	0.052	0	0	0	0.045	0	0	0.132	0	0	0.057	0	0.045	0	0	0	0.09

In PCCS implementations before Revision 3 of this report, only the historic covariance matrix was employed. However, since compositions during operation may differ significantly from the historical mean composition used to define $\mathbf{S}_m$, the variance estimates using the historic covariance matrix may not adequately describe the measured molar oxide concentrations in $\underline{z}$.

Therefore to better represent the true composition and covariances for the current SME batch, starting with Revision 3, the averaged measured elemental composition, $\underline{x}_n$, was used to estimate a covariance matrix based upon these n sample measurements, $\mathbf{S}_n$. This is accomplished by substituting the i^{th} member of the measured elemental composition, $(\underline{x}_n)_i$, for $\bar{x}_i$ in the above covariance matrix definition:

Equation 131

$$(\mathbf{S}_n)_{i,j} = \left[\left(\frac{\gamma_i}{M_i}\right)(r_m)_i(\underline{x}_n)_i\right]\left[\left(\frac{\gamma_j}{M_j}\right)(r_m)_j(\underline{x}_n)_j\right]\rho_{i,j}$$

Since sufficient information does not exist to determine the exact nature of the analytical errors, both covariance matrices, i.e., $\mathbf{S}_m$ and $\mathbf{S}_n$, will be computed along with their impact on the corresponding property variances. The proper test is that based upon the larger resulting property variance.

The tests for measurement acceptability will be defined that use the covariance matrices just determined. If the average measurement $\underline{z}_n$ is distributed in probability as *multivariate* Gaussian around its true value $\underline{\mu}$ with covariance $\left(\frac{\mathbf{\Sigma}}{n}\right)$, then a linear form $\left(\underline{z}_n\underline{a}^T\right)$ is distributed as *univariate* Gaussian [43] with mean $\left(\underline{\mu}\underline{a}^T\right)$ and variance $\left(\frac{\underline{a}\mathbf{\Sigma}\underline{a}^T}{n}\right)$. One consequence of this is that the statistics [44]:

$$\frac{\underline{z}_n\underline{a}^T - \underline{\mu}\underline{a}^T}{\sqrt{\frac{\underline{a}\mathbf{S}_m\underline{a}^T}{n}}} \qquad \text{and} \qquad \frac{\underline{z}_n\underline{a}^T - \underline{\mu}\underline{a}^T}{\sqrt{\frac{\underline{a}\mathbf{S}_n\underline{a}^T}{n}}}$$

are each distributed as a Student's t with (m–1) degrees of freedom, where n is the number of samples on which $\underline{z}_n$ is determined, $\mathbf{S}_m$ is the previous sample estimate of $\mathbf{\Sigma}$ based on m historic observations and their average, and $\mathbf{S}_n$ is a sample estimate of $\mathbf{\Sigma}$ based upon the historic correlation information and the average of the current SME measurements.

Furthermore the number of historical analyses, m, necessary to define reasonable estimates of the pair-wise correlations increases as the number of individual elements increases.[†] For the DWPF prototypic information, only 22 measured compositions are available to estimate the historic SME covariance matrix for the 15 elements of interest for Waste Qualification Runs and Radioactive startup.[††] This number of points appears small when compared to the desired number (i.e., approximately 45), but reasonable to estimate variances for individual elements.

[†] A reasonable rule-of-thumb is that at least three times the number of individual elements are necessary to estimate reasonable correlations. Likewise, 10 points are normally sufficient to reasonably estimate the variance (i.e., $s_{i,i}$) for an individual parameter.

[††] A total of 24 measured compositions were originally available to estimate the covariance matrix; however, two were later omitted as outliers [45, 46].

The ramification of using such a relatively small sample size is that the correlations (but not the variances) may be poorly estimated. The correlations estimated from the 22 historic, prototypic SME measurements are provided in Table B1 of Appendix B. However, since most of the correlations are large and positive (e.g., $\rho_{Al,Ca} = 0.90$, $\rho_{Al,Fe} = 0.93$, $\rho_{Al,Si} = 0.69$, etc.), it would be difficult to imagine that the correlation estimates from a larger sample set would be appreciably larger than those in Table B1.† If the correlations are generally smaller, then the variance estimated would also generally be smaller and the current estimates would be conservative.

For a constraint (call it constraint i) that may be expressed as a linear combination (through vector $\underline{a}_i$) of the average molar oxide concentrations (the $\underline{z}$ vector), the measurement error variance may be represented by $V\left[\underline{z}_n(\underline{a}_i)^T\right]$, where the appropriate variance will be the maximum of the variances associated with the historic covariance matrix and the covariance based upon the current sample measurement:

Equation 132

$$V\left[\underline{z}_n(\underline{a}_i)^T\right] \equiv \max imum\left[\begin{array}{l}\dfrac{(\underline{a}_i)\mathbf{S}_m(\underline{a}_i)^T}{n} = \dfrac{1}{n}\displaystyle\sum_{j=0}^{q-1}\sum_{k=0}^{q-1}(\underline{a}_i)_j(\underline{a}_i)_k(\mathbf{S}_m)_{j,k} \\ \dfrac{(\underline{a}_i)\mathbf{S}_n(\underline{a}_i)^T}{n} = \dfrac{1}{n}\displaystyle\sum_{j=0}^{q-1}\sum_{k=0}^{q-1}(\underline{a}_i)_j(\underline{a}_i)_k(\mathbf{S}_n)_{j,k}\end{array}\right]$$

Thus, the MU for this i^{th} constraint, MU_i, may be computed using:

Equation 133

$$MU_i \equiv t_\alpha(m-1)\sqrt{V\left[\underline{z}_n(\underline{a}_i)^T\right]}$$

where, as previously stated, $t_\alpha(m\text{-}1)$ is the upper $100\alpha\%$ tail of the Student's t distribution with m-1 degrees of freedom. In this situation, m=22, so the appropriate t statistic for a 95% confidence level is $t_{0.05}(21) = 1.721$. If, at management's discretion, the MU is to be accounted for at a lower confidence level for a non-waste-affecting constraint, it can be accomplished through this t statistic. Increasing α above 0.05 correspondingly reduces the confidence associated with the handling of the MU.

To complete the MAR assessment of the i^{th} constraint, combine the offset, $ß_i$, (appropriately adjusted for any applicable property model uncertainty) and the MU (developed above) into the constraint inequality as given by Equation 2 in the body of this report to obtain:

Equation 134

$$\underline{z}_n(\underline{a}_i)^T - ß_i - MU_i \geq 0$$

This inequality defines the MAR for the i^{th} constraint. The overall acceptability MAR is defined by the confluence of all of the MAR results representing the individual constraints. A SME composition must be proven interior to all such constraint regions to be adjudged acceptable. There is thus the concomitant possibility that the simultaneous application of many such tests might cause the false-reject rate to be too high, that is, if these tests are independent. However, only the constraints for B, Li, and Na PCT releases must be controlled to a high degree of certainty [4]; furthermore, these tests are in no way independent as they are all based upon ΔG_p [3] and [14]. Finally the results from DWPF Waste Qualification testing [3]

† At least, it is difficult to imagine that revised correlations would have a significant impact on the property variances computed from the resulting covariance matrices.

and the DWPF operations illustrate that the simultaneous application of all constraints for process and product control does not cause the false-reject rate to burgeon. Thus the MU outlined in this appendix can be applied as indicated; however, if problems concerning the false-reject rate are noticed in future DWPF operation, techniques are available to correctly account for the simultaneous application of constraints.

Distribution:

a.fellinger@srnl.doe.gov
aaron.staub@srs.gov
alex.cozzi@srnl.doe.gov
Alexander Choi/SRNL/Srs
Amanda Shafer/SRR/Srs
Azadeh Samadi-Dezfouli/SRR/Srs
barbara.hamm@srs.gov
Bernard Enevoldsen/SRR/Srs
Bill Holtzscheiter/SRR/Srs
Bill.Brasel@parsons.com
bill.wilmarth@srnl.doe.gov
Boyd.Wiedenman@srnl.doe.gov
Brad.Swanson@parsons.com
cameron.sherer@srnl.doe.gov
Carol Jantzen/SRNL/Srs
Charles Crawford/SRNL/Srs
Chris Martino/SRNL/Srs
Christie.sudduth@srs.gov
Cj Bannochie/SRNL/Srs
cliff.conner@parsons.com
Connie Herman/SRNL/Srs
Cory Trivelpiece/SRNL/Srs
Dan Lambert/SRNL/Srs
daniel.mccabe@srnl.doe.gov
David Dooley/SRNL/Srs
David Newell/SRNL/Srs
david.crowley@srnl.doe.gov
david.herman@srnl.doe.gov
Devon McClane/SRNL/Srs
Earl Brass/SRR/Srs
Elizabeth Hoffman/SRNL/Srs
Eric Freed/SRR/Srs
erich.hansen@srnl.doe.gov
Fabienne Johnson/SRNL/Srs
Frank Pennebaker/SRNL/Srs
geoffrey.smoland@srnl.doe.gov
Hasmukh Shah/SRR/Srs
Helen Boyd/SRR/Srs
Jack Zamecnik/SRNL/Srs
Jake Amoroso/SRNS/Srs
james.folk@srs.gov
Jamie Babcock/SRR/Srs
jean.ridley@srs.gov
Jeff Ray/SRR/Srs
Jeffrey Gillam/SRR/Srs
jeffrey.crenshaw@srs.gov
Jeremiah Ledbetter/SRR/Srs
Jocelyn.Lampert@srnl.doe.gov
John Iaukea/SRR/Srs
John Pareizs/SRNL/Srs
John Schwenker/SRR/Srs
John Windham/SRR/Srs
john.mayer@srnl.doe.gov
Jonathan Bricker/SRR/Srs
Kevin Brotherton/SRR/Srs
Kevin Fox/SRNL/Srs
Kevin.Kostelnik@srs.gov
Lauryn Jamison/SRR/Srs
luke.reid@srnl.doe.gov
Michael Stone/SRNL/Srs
michael.broome@srs.gov
michael.cercy@srnl.doe.gov
Michael.norton@srs.gov
Noel Chapman/SRR/Srs
Patricia.suggs@srs.gov
patrick.jackson@srs.gov
paul.ryan@srs.gov
Richard Edwards/SRR/Srs
roberto.gonzalez@srs.gov
Ryan McNew/SRR/Srs
Ryan.Lentsch@gat.com
Samuel Fink/SRNL/Srs
Skip.Singer@parsons.com
Susan Lawson/SRR/Srs
Terri Fellinger/SRR/Srs
thelesia.oliver@srnl.doe.gov
Timothy Brown/SRNL/Srs
Tom.Burns@parsons.com
Tommy Edwards/SRNL/Srs
tony.polk@srs.gov
Victoria Kmiec/SRR/Srs
Vijay Jain/SRR/Srs
William.Ramsey@SRNL.DOE.gov